

Response to Associate Editor Comments
(G. Gehrels, 10 July, 2020)

Blue = AE comments from 26 March 2020

Green = AE comments from 17 June 2020

Black = author response to comments

Red = changes to manuscript

Responses to the AE comments are inserted below.

Sharman Review:

1. Dr. Sharman gave a positive review that raises one major point and several minor ones. The major concern was about the lack of evidence to support the inference that near depositional age zircon is air-fall in origin and older zircon is recycled. You responded to this comment by saying that you are:

unable to provide reliable information about morphology of the young grains, as most were plucked out from the mounts and dissolved for CA-TIMS geochronology. We tried to do this analysis with BSE images of the grains (before analysis), but the size/shape of the grains in the images has little bearing on the true size/shape of the grains. This because the mounts were polished down just a little so as to retain more material for the CA-TIMS analyses.

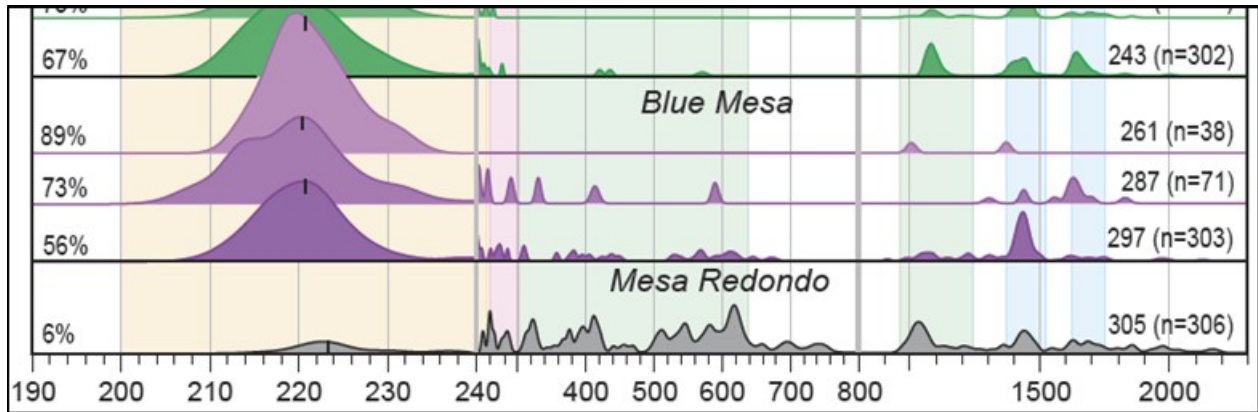
I would have thought that even a two-dimensional cross section through a c-axis parallel zircon grain would reveal whether the grain is prismatic or not. If you have stored the BSE images, then I would encourage you to include them in an online data repository.

Response: We would love to be able to provide this info, as it would be great test of our interpretations concerning air-fall versus detrital zircons. Unfortunately, we just can't extract reliable information from the BSE images because the mounts were polished down just far enough to expose a little bit of each crystal. It's just not possible to say anything reliable about grain shape from the BSE images. We also are unable to go back and look at the grains in the mounts as many have been removed from the mount for CA-TIMS analysis.

2. The reviewer also has a question about the change in scale of your age distributions. An alternative way to bump the height of the pre-240Ma age component would be to plot the age distributions on a logarithmic time scale. Furthermore, if you replace your Probability Density Plots (PDPs) by Kernel Density Estimates (KDEs), then you can tweak their bandwidth to produce the most informative result. As you know, cumulative distributions are also useful for data visualization. They, too, can be plotted on a logarithmic time axis.

PDP vs KDE: I won't fight with you over this. If you want to use PDPs to visualise your data then that is fine with me. But please don't use them for quantitative analysis.

Response: Indeed, there are several different options for showing the age distributions, and we have experimented with a few. In our view, none of the other options (e.g., log scale or cumulative plots) show the details of the Triassic ages, and the proportions and ages of the older components, as clearly as the current plot (a portion of which is shown below).



Response: Ages distributions remain as PDP's, quantitative analyses are now conducted with KDE's.

Ramezani Review:

1. Stratigraphy: Dr Ramenazi is concerned that the observed drift between your MDAs and the depositional ages is due to misidentification of the stratigraphic positions in the CPCP core. In your response, you wrote that your paper does not aim to present an age model, and does not claim to estimate accurate MDAs either. I am a bit confused, because the paper does seem to me like an attempt to calibrate the depositional history of the CPCP core in absolute time. If your paper has a different objective, then please state more clearly what the purpose of the study actually is. I apologise if I am missing something obvious here.

Age models: I won't fight over this either. I understand that you don't present a new age model. But what then is the purpose of the MDA estimates?

Correct, LA-ICPMS data are not used to construct an age model. The age model shown is based on magnetostratigraphy (Kent et al., 2019), with constraints from CA-TIMS (Rasmussen et al., 2020).

The purpose of the MDA's is to provide an estimate of the age of the main cluster of dates from each sample. Comparison of these MDA's with the age model yields two conclusions of geological significance:

First, MDA's overlap with the age model for fine-grained strata but are a few m.y. older for coarse-grained strata. This is interpreted to record the presence of mainly air-fall (depo-age) zircons in the fine-grained strata, whereas coarser-grained strata are dominated by older/recycled grains.

Second, MDA's for sandstones are similar for tens of meters of stratigraphy, whereas the age model youngs upward (of course). This provides interesting information about patterns of recycling of older grains in the Chinle fluvial system.

2. U-Pb geochronology: Dr. Ramenazi is concerned that the LA-ICP-MS results may be affected by Pb-loss, which would invalidate their use as maximum depositional ages. In your response, you write that:

This manuscript goes to great length to document that Pb loss is a significant factor for many of the grains analyzed. We show this internally with the Uconce tests described above. We also document this by comparison of our ages with the CA-TIMS data from the same grains (Appendix 2). Indeed, Pb loss is an important factor for many of our analyses! But the assertion that LA-ICPMS max depo ages are younger than the CA-TIMS ages of Ramezani et al. (2011) and Atchley et al. (2013) due to Pb loss is not supported by the fact that most of the reported LA-ICPMS MDA's are older (not younger) than the equivalent MDA's reported by R+2011 and A+ 2013!!

Appendix 2 clearly shows that the LA-ICP-MS data are consistently 5-10 Ma younger than the CA-TIMS ages. To me this confirms the reviewer's concerns. The fact that the ad-hoc MDA estimates for the youngest LA-ICP-MS peak (which are shown as circles in Appendix 2) are consistently older than the CA-TIMS estimates (which are shown as red bars in Appendix 2) is a result of comparing datasets of different size. Your LA-ICP-MS based MDA estimate uses more grains than the CA-TIMS estimate, making the comparison between the two estimates biased. This problem is diagnostic of a fundamental flaw in three of the four MDA estimation algorithms that are proposed in the manuscript. I will discuss this in more detail below.

Maximum depositional ages: it would be great if you could give the Galbraith approach a try. If you like it then that would solve this issue.

I have used the RadialPlotter routine in IsoplotR to calculate Minimum Ages for all samples. The results are reported in Table 6, shown on Figures 5 and 13 and Appendix 2, and discussed in the revised text. These are interpreted to represent the most reliable Max Depo Age for each sample.

The manuscript has been revised to present minimum ages for all samples, and to explore the implications of the patterns of these ages for the present data set and for the utility of the minimum age model.

Further Comments:

1. The paper uses four different heuristic MDA estimation algorithms. Three of these methods are problematic, because they drift to ever younger ages with increasing sample size.

(a) Age of the youngest peak on a probability density plot (PDP): PDPs have no statistical basis, and any quantitative information derived from them is of dubious statistical significance. If you were to analyse one million grains of zircon, then the youngest age cluster on a PDP would likely be younger than the actual depositional age.

(b) Weighted Mean age and uncertainty of the youngest cluster: Same problem. Any heuristic method that is based on p-values is problematic because p-values are a sensitive function of sample size. The larger the sample size, the greater the likelihood that the χ^2 -test identifies spurious peaks.

(c) Maximum Likelihood age and uncertainty. See Figure 6.3 of Vermeesch (2018b) for an example of how multimodal unmixing models suffer from the same problem as methods a. and b.

The sample size dependency is actually reported in the paper (“Ironically, the more grains analyzed, the greater the inaccuracy of [the] youngest age!”). I do not understand why these broken methods are still used in the paper and would advocate that they are removed. In statistics, it is desirable for estimates to asymptotically converge to the truth with increasing sample size. Only the Tuffzirc age model may have this property. An alternative would be the parametric minimum age model of Galbraith and Laslett (1993). But neither of these techniques is immune to the Pb-loss problem.

Maximum depositional ages: it would be great if you could give the Galbraith approach a try. If you like it then that would solve this issue.

We have addressed these comments in two ways:

1. To represent the AE's concerns about the statistical validity of these methods, we have noted in the Analytical Methods section that Vermeesch (2018b) has documented issues with the robustness of all of these methods.

2. As noted above, we have applied the minimum age model, and it provides a more reliable MDA for most samples.

The revised text explores all of these issues, and concludes with a discussion of the power of the minimum age method for addressing both simple and complex age distributions.

2. The paper frequently uses two ad-hoc dissimilarity measures called ‘Likeness’ and ‘Cross-correlation Coefficient’ (CCC). These quantities are both derived from PDPs and are flawed for

reasons that are given in detail by Vermeesch (2018a). Please remove these from the paper and replace them with bona fide statistical dissimilarity measures such as the Kolmogorov-Smirnov statistic. Of course, if you can present a statistically valid argument against my objections to Likeness and CCC, then I would be happy to change my mind.

Likeness and cross correlation: here I am going to stand my ground.

Done -- Likeness, Similarity, and Cross Correlation these have been removed!

Statistical comparisons using Likeness, Similarity, and Cross Correlation have been removed. All discussion of these methods has been removed. DR Tables 4 and 5 now report comparisons using KS-D values and Kuiper-V values.

MDS plots (Figures 9 and 11) have been remade using KS-D values.

3. Is Figure 10 a two-dimensional PDP or KDE? I think that this diagram would be more effective as a contour plot, or as a simple scatter plot. The three-dimensional effect adds no useful information.

Response: These are based on two-dimensional KDE's. With regard to the 3-d effect, I think this helps readers evaluate similarities/differences of the various units.

1 **LA-ICPMS U-Pb geochronology of detrital zircon grains from the Coconino,**
2 **Moenkopi, and Chinle Formations in the Petrified Forest National Park (Arizona)**

3
4
5 George Gehrels¹, Dominique Giesler¹, Paul Olsen², Dennis Kent³, Adam Marsh⁴, William Parker⁴,
6 Cornelia Rasmussen⁵, Roland Mundil⁵, Randall Irmis⁶, John Geissman⁷, and Christopher Lepre³

7 ¹Department of Geosciences, University of Arizona, Tucson AZ 85721, USA

8 ²Lamont-Doherty Earth Observatory of Columbia University, Palisades, NY 10964, USA

9 ³Earth and Planetary Sciences, Rutgers University, Piscataway, NJ 08854, USA

10 ⁴Petrified Forest National Park, Petrified Forest, AZ 86028, USA

11 ⁵Berkeley Geochronology Center, 2455 Ridge Rd., Berkeley CA 94709, USA

12 ⁶Natural History Museum of Utah and Department of Geology & Geophysics,

13 University of Utah, Salt Lake City, UT 84108, USA

14 ⁷Department of Geosciences, University of Texas at Dallas, Richardson, TX 75080, USA

15
16
17
18
19
20 *Correspondence to George Gehrels (ggehrels@gmail.com)*

21 ~~8-Sept-2019~~10 July 2020 draft; re-submitted to Geochronology

22 *(revised to accommodate review and AE comments)*

23 **ABSTRACT**

24 U-Pb geochronology was conducted by Laser Ablation-Inductively Coupled Plasma Mass
25 Spectrometry (LA-ICPMS) on 7,175 detrital zircon grains from twenty-nine samples from the
26 Coconino Sandstone, Moenkopi Formation, and Chinle Formation. These samples were
27 recovered from ~520 m of drill core that was acquired during the Colorado Plateau Coring
28 Project (CPCP), located in Petrified Forest National Park (Arizona).

29 A sample from the lower Permian Coconino Sandstone yields a broad distribution of
30 Proterozoic and Paleozoic ages that are consistent with derivation from the Appalachian and
31 Ouachita orogens, with little input from local basement or Ancestral Rocky Mountain sources.
32 Four samples from the Holbrook Member of the Moenkopi Formation yield a different set of
33 Precambrian and Paleozoic age groups, indicating derivation from the Ouachita orogen, the
34 East Mexico Arc, and the Permo-Triassic arc built along the Cordilleran margin.

35 Twenty-three samples from the Chinle Formation contain variable proportions of Proterozoic
36 and Paleozoic zircon grains, but are dominated by Late Triassic grains. LA-ICPMS ages of these
37 grains belong to five main groups that correspond to the Mesa Redondo Member, Blue Mesa
38 Member and lower part of the Sonsela Member, upper part of the Sonsela Member, middle
39 part of the Petrified Forest Member, and upper part of the Petrified Forest Member. The ages
40 of pre-Triassic grains also correspond to these chronostratigraphic units, and are interpreted to
41 reflect varying contributions from the Appalachian orogen to the east, Ouachita orogen to the
42 southeast, Precambrian basement exposed in the Ancestral Mogollon Highlands to the south,
43 East Mexico arc, and Permian-Triassic arc built along the southern Cordilleran margin. Triassic
44 grains in each chronostratigraphic unit also have distinct U and Th concentrations, which are
45 interpreted to reflect temporal changes in the chemistry of arc magmatism.

46 Comparison of our LA-ICPMS ages with available CA-TIMS ages and new magnetostratigraphic
47 data provides new insights into the depositional history of the Chinle Formation, as well as
48 methods utilized to determine depositional ages of fluvial strata. For parts of the Chinle
49 Formation that are dominated by fine-grained clastic strata (e.g. mudstone and siltstone), such
50 as the Blue Mesa Member and Petrified Forest Member, all three chronometers agree (to
51 within ~1 m.y.), and robust depositional chronologies have been determined. In contrast, for
52 stratigraphic intervals dominated by coarse-grained clastic strata (e.g., sandstone), such as
53 most of the Sonsela Member, the three chronologic records disagree due to recycling of older
54 zircon grains and variable dilution of syn-depositional-age grains. This results in LA-ICPMS ages
55 that significantly pre-date deposition, and CA-TIMS ages that range between the other two
56 chronometers. These complications challenge attempts to establish a well-defined
57 chronostratigraphic age model for the Chinle Formation, ~~and to evaluate possible connections~~
58 ~~among fundamental Late Triassic biotic and climatic changes and a red siliceous horizon~~
59 ~~encountered in the CPCP core.~~

60 1. INTRODUCTION

61 Triassic strata of the Colorado Plateau and environs provide rich and geographically extensive
62 records of environmental and biotic change during a critical period of Earth history, as well as
63 the transition from passive- to convergent-margin tectonism along the North American
64 Cordillera (e.g., Parker and Martz, 2011; Olsen et al., 2011). As demonstrated by Riggs et al.
65 (1996, 2003, 2012, 2013, 2016), Dickinson and Gehrels (2008), Irmis et al. (2011), Ramezani et
66 al. (2011, 2014), Atchley et al. (2013), Nordt et al. (2015), Kent et al. (2018, 2019), Olsen et al.
67 (2018, 2019), Marsh et al. (2019), and Rasmussen et al. (202019), Chinle Formation strata have
68 the potential to record the timing of these changes in great detail given their several-hundred-
69 meter thickness, abundance of near-depositional-age zircon grains, and recoverable
70 paleomagnetic reversal stratigraphy.

71 In an effort to further develop this record, ~520 m of continuous core was collected from
72 Triassic and underlying Permian strata at Petrified Forest National Park (PEFO), which is located
73 on the southern Colorado Plateau of northern Arizona (Fig. 1; [\(35.085933° N, 109.795500° W,](#)
74 [WGS84 datum](#)). The objectives and primary findings of this project have been described by
75 Olsen et al. (2018, 2019), Kent et al. (2018, 2019), and Rasmussen et al. (202019), and
76 numerous related studies are currently in progress. This contribution to the project reports ~~on~~
77 U-Pb geochronologic analyses of detrital zircon grains that were extracted from twenty-nine
78 samples from this core (CPCP-PFNP13-1A). Analyses were conducted by laser ablation-
79 inductively coupled mass spectrometry (LA-ICPMS), with between 36 and 490 grains analyzed
80 per sample ([total of 7,175 analyses](#)). Grains were chosen for analysis by random selection in an
81 effort to provide unbiased information about provenance. Fortunately, a significant number of
82 near-depositional-age grains were recovered from many samples in the Chinle Formation,
83 which provides opportunities to also determine robust maximum depositional ages. This report
84 explores variations in both provenance and maximum depositional age of strata intersected in
85 the CPCP-PFNP13-1A core, and the implications for Permian-Triassic environmental and biotic
86 transformations and the tectonic evolution of southwestern North America.

87 2. STRATA ENCOUNTERED IN THE PETRIFIED FOREST NATIONAL PARK DRILL CORE

88 The lowest stratigraphic horizon encountered consists of quartz arenite belonging to the
89 Coconino Sandstone (Fig. 2). This unit belongs to regionally extensive erg deposits of early
90 Permian (Leonardian) age (Blakey et al., 1988; Lawton et al., 2015; Dickinson, 2018).

91 Overlying strata of the Coconino Sandstone are tabular, thin to thick-bedded, reddish
92 mudstone, siltstone, and sandstone layers of the Lower-Middle Triassic Moenkopi Formation. In
93 the PEFO region, the Moenkopi Formation consists of thin-bedded reddish siltstone with
94 interlayered sandstone and mudstone. Lower, finer-grained strata are assigned to the Wupatki
95 Member and Moqui Member, and upper sandstone-rich horizons dominate the Holbrook
96 Member. The base is a regional unconformity, the TR-1 unconformity of Pipiringos and
97 O'Sullivan (1978), along which strata of the lower Permian Toroweap Formation and Kaibab

98 Formation have been removed. Strata of the Moenkopi Formation are interpreted to have
99 accumulated on a northwest-sloping coastal plain, with thinner fluvial strata to the southeast
100 and thicker marginal marine strata to the northwest (Dickinson, 2018). The Moenkopi
101 Formation basin was bounded by residual uplifts of the Ancestral Rocky Mountains to the
102 northeast and highlands of the Ouachita orogen to the southeast. Highlands developed within
103 early phases of the Cordilleran magmatic arc may have existed to the southwest.

104 Strata of the Moenkopi Formation are overlain unconformably [Tr-3 unconformity of Pippingos
105 and O'Sullivan (1978)] by the Chinle Formation (Fig. 2). The transition is marked in most areas
106 by the Shinarump Conglomerate, which consists of cobbles of chert, quartzite, limestone and
107 subordinate felsic volcanic rocks. Riggs et al. (2012) have determined U-Pb ages of 232-224 Ma
108 on volcanic cobbles in the Shinarump Conglomerate. The Shinarump Conglomerate is
109 interpreted to correlate with finer-grained strata of the Mesa Redondo Member (Irmis et al.,
110 2011; Martz et al., 2012, 2017; Riggs et al., 2016). Strata of the Shinarump Conglomerate and
111 Mesa Redondo Member are interpreted to have accumulated in paleovalleys that were carved
112 into underlying strata. Strikingly variegated, strongly pedogenically modified, red, purple, and
113 yellow strata in the core are assigned to the Mesa Redondo Member given the lack of
114 conglomerate. Strata of the Mesa Redondo Member in outcrop have yielded U-Pb (~~U-Pb~~ zircon)
115 ages of ~227.6 Ma (Atchley et al., 2013) and ~225.2 Ma (Ramezani et al., 2011).

116 Gradationally overlying the Mesa Redondo Member are strata of the Blue Mesa Member,
117 which consist of purplish to gray and red bentonitic mudstone with sandstone beds that are
118 generally 0.5 m in thickness (Woody, 2006). Blue Mesa Member mudstones are pervasively
119 pedogenically modified in the core. These strata are interpreted to have accumulated primarily
120 as overbank deposits within a mixed-load meandering river system (Martz and Parker, 2010).
121 Previously reported U-Pb (ID-TIMS or CA-TIMS) ages from outcrop of the Blue Mesa Member
122 range from ~223 Ma to ~218 Ma (Heckert et al., 2009; Ramezani et al., 2011; Irmis et al., 2011;
123 Atchley et al., 2013; Rasmussen et al., ~~2019~~).

124 Strata of the Blue Mesa Member are overlain by sandstone-rich and conglomerate-bearing
125 strata of the Sonsela Member. Lucas (1993) and Heckert and Lucas (2002) refer to the base of
126 the Sonsela Member as a regionally significant unconformity, although this interpretation has
127 been questioned by Woody (2006) and Martz and Parker (2010) given that conglomeratic
128 sandstone of the Sonsela is interbedded with mudstone of the Blue Mesa Member. Martz and
129 Parker (2010) suggest that the transition from the Blue Mesa Member to the Sonsela Member
130 marks a change in depositional regime (from mainly overbank deposits to bedload-dominated
131 channel deposits) but does not mark a significant hiatus in deposition.

132 The Sonsela Member consists predominantly of sandstone with lesser mudstone and local
133 conglomerate. Sandstone beds are variable in thickness, have significant lateral extent, and
134 exhibit cut-and-fill structure (Woody, 2006). Conglomerate (with abundant volcanic clasts) is
135 common within the sandstone beds. Five units have been recognized, a lower sandstone
136 interval (Camp Butte beds), a lower-middle unit with abundant mudstone (Lot's Wife beds), a

137 middle sandstone and conglomerate unit (Jasper Forest/Rainbow Forest bed), a middle-upper
138 unit with pedogenic carbonate and abundant mudstone (Jim Camp Wash beds), and an upper
139 sandstone unit (Martha's Butte beds) (Martz and Parker, 2010). The five units are gradational,
140 with the main variation being the abundance of mudstone in two of the middle units. A reddish
141 siliceous horizon of uncertain regional extent has been recognized within the middle of the
142 upper mudstone-rich unit in the CPCP-PFNP13-1A core. Similar horizons within other exposures
143 of the Sonsela Member are marked by a significant die-off of the conifers that characterize
144 Petrified Forest National Park (Creber and Ash, 1990), a turn-over of the vertebrate fauna
145 (Parker and Martz, 2009, 2011), and perhaps a significant change in flora and paleoclimate
146 (Reichgelt et al., 2013; Nordt et al., 2015; Baranyi et al., 2017). U-Pb (CA-TIMS/zircon) ages from
147 the Sonsela Member range from ~220 to ~214 Ma (Ramezani et al., 2011; [Marsh et al., 2019](#);
148 [Rasmussen et al., 202019](#)) from below the siliceous horizon and from ~214 to ~213 Ma
149 (Ramezani et al., 2011; Nordt et al., 2015; Kent et al., 2018; [Rasmussen et al., 202019](#)) from
150 above.

151 Overlying the conglomeratic sandstones of the Sonsela Member is a purplish mudstone that
152 marks the base of the Petrified Forest Member (Fig. 2). This member consists of red and purple
153 mudstone with abundant paleosols and pedogenic carbonate nodules, with local conglomeratic
154 sandstone beds that formed in bedload-dominated streams. Near the top of the unit is the
155 Black Forest bed, which consists of limestone-pebble conglomerate and reworked andesitic tuff
156 (Ash, 1992). Zircon grains from the Black Forest bed have yielded U-Pb (ID-TIMS or CA-TIMS)
157 ages of ~213 Ma to ~210 Ma (Riggs et al., 2003; Heckert et al., 2009; Ramezani et al., 2011; Kent
158 et al., 2018; [Rasmussen et al., 202019](#)).

159 **3. SAMPLED HORIZONS**

160 We analyzed detrital zircon grains from twenty-nine samples collected from the Permian and
161 Triassic strata described above. Samples include one from the Coconino Sandstone, five from
162 the Moenkopi Formation (one that may be from the Wupatki Member and four from the
163 Holbrook Member), and twenty-three from the Chinle Formation (one from the Mesa Redondo
164 Member, three from the Blue Mesa Member, twelve from the Sonsela Member, and seven
165 from the Petrified Forest Member). Approximate stratigraphic positions of the samples are
166 shown on Figure 2, lithic characteristics are described in DR Table 1, and images of the sampled
167 material (both core and thin sections) are presented in Appendix 1. Each sample consisted of 20
168 cm (for sandstone) to 30 cm (for mudstone-siltstone) of $\frac{1}{4}$ sections of the core.

169 **4. ANALYTICAL AND INTERPRETIVE METHODS**

170 Zircon mineral separation was performed at the Arizona LaserChron Center
171 (www.laserchron.org) using methods modified from those outlined by Gehrels (2000), Gehrels
172 et al. (2008), and Gehrels and Pecha (2014) because of the small size of all samples and the
173 abundance of clay minerals in many samples. The process included using a hand-crusher to
174 break the samples apart, a gold pan for initial density separation, and an ultrasonic disruptor

175 (Hoke et al., 2014) to separate zircon crystals from clay mineral grains. Magnetic separation was
176 performed with a Frantz Isodynamic separator, followed by density separation using methylene
177 iodide.

178 Zircon grains greater than 60 μm in size were enclosed in 1-inch epoxy mounts along with
179 fragments of zircon standards SL (primary) and FC-1 and R33 (secondary). Mounts were
180 polished approximately 5-10 μm deep to expose the internal structure of the grains but retain
181 as much material as possible for subsequent CA-TIMS analysis. Imaging was performed with a
182 backscatter electron detector system (BSE) using a Hitachi S3400 scanning electron microscope
183 (SEM) to ensure analysis of zircon and to avoid inclusions and fractures. Mounts were cleaned
184 with 1% HCl and 1% HNO_3 prior to isotopic analysis.

185 U-Pb isotopic analyses were conducted by LA-ICPMS using a Teledyne/Photon Machines
186 Analyte G2 laser connected to a Thermo Element2 mass spectrometer. Analyses utilized a 20
187 μm diameter laser beam fired at 7 hz for 15 seconds, resulting in 10-12 μm deep pits. Details of
188 the analytical methods are reported in DR Table 2.

189 U-Pb ages are calculated with an in-house data-reduction routine (E2agecalc) following
190 methods of Pullen et al. (2018). Analyses of zircon grains from our samples are reported in DR
191 Table 3, with results filtered for discordance (using cutoffs of 80% and 105% concordance),
192 precision (10%), and common Pb (>600 cps counts of 204). Following the recommendations of
193 Horstwood et al. (2016), uncertainties for individual analyses include only internal (random or
194 measurement) uncertainty contributions, whereas uncertainties of pooled ages contain both
195 internal and external (systematic) contributions.

196 Detrital age distributions are displayed and analyzed with normalized probability density plots,
197 which are based on the individual ages and measured uncertainties from each sample.
198 Provenance interpretations are based on the main clusters of ages, with less emphasis on ages
199 that do not belong to clusters given the possibility that they are unreliable due to Pb loss,
200 inheritance, analysis of inclusions, high common Pb, or unusual Pb/U fractionation due to
201 ablation along fractures (Gehrels, 2014).

202 Analysis of provenance is conducted by comparison with age distributions from five likely
203 source regions for Permian-Triassic strata of the Colorado Plateau, which include the
204 Appalachian orogen, the Ouachita orogen, local basement rocks of southwestern Laurentia, the
205 East Mexico arc, and the Permian-Triassic magmatic arc developed along the Cordilleran margin
206 of southwestern North America (Fig. 1; Dickinson, 2018). The age distributions for these regions
207 include data from: (1) upper Paleozoic strata of the Appalachian foreland basin (Thomas et al.,
208 2017) and Illinois and Forest City basins (Kissock et al., 2018), (2) upper Paleozoic strata of the
209 Delaware (Xie et al., 2018), Fort Worth (Absalem et al., 2018), and Marathon (Thomas et al.,
210 2019) basins, (3) lower Paleozoic strata of the Grand Canyon (Gehrels et al., 2011) and
211 Cordilleran passive margin strata in southern California and northern Sonora (Gehrels and
212 Pecha, 2014), (4) Permian and Triassic strata of the Barranca and El Antimonio Formations of

213 Sonora (Gonzalez-Leon et al., 2009; Gehrels and Pecha, 2014), Jura-Cretaceous strata of the
214 Great Valley (DeGraaff-Surpless et al., 2002; Surpless et al., 2006; Wright and Wyld, 2007),
215 Permian-Triassic igneous rocks in California (Chen and Moore, 1982; Miller et al., 1995; Tobisch
216 et al., 2000; Barth and Wooden, 2006, 2011, 2013; Saleeby and Dunne, 2015), and (5) Mesozoic
217 strata that accumulated adjacent to the East Mexico arc (Ortega-Flores et al., 2014). Age
218 distributions for these five regions are presented in Figure 3.

219 Comparisons of age distributions are quantified using ~~several~~ two different statistical measures
220 that examine the degree to which age distributions contain similar proportions of similar age
221 groups. ~~Five metrics~~ used in this study include the ~~cross-correlation coefficient, values of~~
222 ~~similarity and likeness, and the~~ Kolmogorov-Smirnov D (K-S-D) values and Kuiper-V values.
223 The statistical basis as well as strengths and limitations of each of these metrics are
224 summarized by Saylor and Sundell (2016) ~~and Wissink et al. (2018), and Vermeesch (2018a)~~.
225 Results from these comparisons are presented in DR Table 4. The interpretations offered below
226 are based on ~~cross-correlation~~ KS-D values ~~coefficients~~, although Kuiper-V values ~~all five metrics~~
227 yield similar results. For both metrics, smaller values indicate a higher degree of similarity of
228 age distributions. Comparisons are also presented visually through the use of multidimensional
229 scaling (MDS) diagrams (Vermeesch, 2013; Saylor et al., 2017; Wissink et al., 2018), which
230 provide a 2-dimensional representation of the differences between multiple age distributions.
231 MDS analyses are ~~also~~ based on KS-D values calculated from kernel density estimates (KDE's) of
232 the age distributions ~~cross-correlation coefficients~~.

233 Maximum depositional ages (MDAs) are estimated from the youngest distinct cluster of ages in
234 each sample (e.g., calculated from the age of the youngest distinct cluster of three or more
235 overlapping ages Dickinson and Gehrels, 2009; Gehrels, 2014). The age of this cluster is
236 estimated using ~~five~~ our different methods, each of which has strengths and limitations.
237 Complications with these methods arise from (1) the need to make unconstrained decisions
238 about which analyses to include or exclude from consideration, (2) the evidence that dates in
239 some clusters have been compromised by Pb loss, resulting in dates that post-date deposition,
240 (3) the evidence that some clusters also contain slightly older recycled grains that pre-date
241 deposition, and (4) issues of statistical robustness for some methods (Vermeesch, 2018b).
242 Following are short descriptions of the five ~~our~~ methods:

243 ~~•, as described below.~~

- 244 • Age of the youngest peak on a probability density plot (PDP). This method is advantageous
245 because no decisions are made about which analyses are included/excluded, but it has the
246 disadvantage that no uncertainty is reported for the peak age.
- 247 • Weighted Mean age and uncertainty of the youngest cluster. This method calculates the
248 average age of a cluster by weighting each analysis according to the inverse-square of its
249 uncertainty. The reported uncertainty relates to the mean age (e.g., standard error of the
250 mean), not the age distribution of constituent analyses (e.g., standard deviation). An
251 advantage of this method is that it also yields a Mean Square of the Weighted Deviates
252 (MSWD), which is an indication of the degree to which the ages belong to a single

253 population (values of ~ 1 or less indicate a single population). A disadvantage of this method
254 is that the investigator must decide which ages are included in the calculation, which leads
255 to the possibility of subjective bias. In this study, clusters include the main set of continuous
256 ages, with boundaries selected at the youngest and oldest gap in ages. This calculation is
257 available from the Weighted Mean function in Isoplot (Ludwig, 2008).

- 258 • Tuffzirc age and uncertainty of the youngest cluster. This method uses the age extractor
259 function in Isoplot (Ludwig, 2008), which identifies the largest cluster of ages that overlap to
260 an acceptable degree (probability-of-fit > 0.05), reports the median value as the most likely
261 age, and uses the range of included ages to calculate an asymmetric uncertainty. The
262 reported uncertainty refers to the median value (not the range of constituent analyses).
263 Excluded ages are interpreted to pre-date the selected cluster (if older), or to be
264 compromised by Pb loss (if younger). This method is advantageous in that no subjective
265 decisions are made about including/excluding ages.
- 266 • Maximum Likelihood age and uncertainty. This method uses a maximum likelihood analysis
267 to determine the gaussian distribution that best fits the youngest cluster. The reported
268 uncertainty refers to the most likely value (not the range of constituent analyses). This
269 method is advantageous in that no subjective decisions are made about including/excluding
270 ages. It is available from the Unmix function of Isoplot (Ludwig, 2008).

271

272 Finally, we also use the minimum age model of Galbraith and Laslett (1993) and Vermeesch
273 (2020). This method assumes that a set of dates is a mixture of a discrete young component
274 and a continuous older component. It uses the method of maximum likelihood to determine
275 the age and uncertainty of the younger component. Calculations were conducted using IsoplotR
276 (Vermeesch, 2018b), which returns the minimum age and also a central age that is similar to
277 the weighted mean described above.

278

279

280 The results of these calculations are presented in DR Tables ~~3 and~~ 6. Shown separately are
281 estimates from the first four methods noted above, and the average of these four estimates, as
282 well as the minimum age (and uncertainty) which we interpret as the maximum depositional
283 age.

284

285 DR Table 6 also reports the age and uncertainty of the youngest analysis from each sample. This
286 youngest age does not provide a reliable maximum depositional age given that the youngest
287 age of a distribution will always be younger than the true age due to analytical uncertainty
288 (Gehrels, 2014). For example, as described by Coutts et al. (2019), consider the analytical data
289 from a population of zircon grains that have exactly the same true age. Because of analytical
290 uncertainty, the measured ages of half of the analyses will be younger than the true age, and
291 half will be older, and the youngest age will be significantly younger than the mean (true) age.
292 Ironically, the more grains analyzed, the greater the inaccuracy of this youngest age
293 (Vermeesch, 2020)!

294 In addition to this statistical bias, the youngest single age will be even farther from the mean
295 (true) age if it has been compromised by Pb loss ([e.g., Andersen et al., 2019](#)). We report these
296 youngest ages because they provide important information about the possibility that analyses
297 included in the youngest cluster have also experienced Pb loss. DR Table 6 accordingly reports
298 this youngest age (and uncertainty), as well as information about its U concentration, the
299 average U concentration of the youngest cluster of ages, and whether the youngest age belongs
300 to the youngest cluster or is an outlier (based on Tuffzirc analysis). U concentration is important
301 because Pb loss is commonly correlated with the degree of radiation damage, which is a
302 function of U concentration (and age).

303 A second test of the likelihood that analyses belonging to the youngest cluster have
304 experienced Pb loss is provided by a plot of U concentration versus age for analyses belonging
305 to the youngest cluster. Such plots are shown for every sample in DR Table 3, and whether a
306 correlation exists is indicated in DR Table 6.

~~307 Also included in DR Table 6 are the preferred MDA age and uncertainty for each sample. The
308 preferred age is based on the average of the four age estimates determined by peak age,
309 weighted mean, Tuffzirc, and Unmix analyses. The uncertainty of this preferred age is based on
310 the average of the uncertainty from each method, and is shown with both internal-only
311 uncertainties and with combined internal and external uncertainties.~~

312 The average precision of individual analyses reported herein is 2.3% (2σ) for $^{206}\text{Pb}^*/^{238}\text{U}$ dates
313 and 2.6% for $^{206}\text{Pb}^*/^{207}\text{Pb}^*$ dates. For pooled ages, calculated as described above, the average
314 precision is 0.52% (2σ) including only internal uncertainties and 0.98% (2σ) including both
315 internal and external sources of uncertainty. The accuracy of our analyses can be estimated
316 from the age of the secondary standards that were analyzed with each set of unknowns. As
317 reported in DR Table 7 and shown on Figure 4, sets of $^{206}\text{Pb}^*/^{238}\text{U}$ dates for FC-1 are offset
318 between +0.25% and -0.45% from the reported $^{206}\text{Pb}^*/^{238}\text{U}$ date of 1099.9 Ma (Paces and
319 Miller, 1993), with an average offset for all 1,065 analyses of +0.03%. For R33, offsets range
320 from +0.85% to -0.95% from the assumed age of 419.3 Ma (Black et al., 2004), with an average
321 offset for all 291 ages of -0.23%. MSWD values for the sets of FC-1 and R33 ages are 0.95 and
322 0.92 (respectively) – this demonstrates that [reported uncertainties for individual analyses are](#)
323 [accurate, and that](#) MSWD values for sets of unknown ages are reliable indicators of the
324 existence of multiple age components.

325 Interpretation of our ages relative to the Geologic Time Scale is based on the August 2018
326 version of the International Chronostratigraphic Chart (Cohen et al., 2013).

327 U-Pb geochronology by LA-ICPMS also provides U concentrations and U/Th values for each
328 analysis, which can be used as a geochemical fingerprint of detrital zircon grains (e.g., Gehrels
329 et al., 2006, 2008; Riggs et al., 2012, 2016). This information is accordingly reported for each
330 analysis in DR Table 3, and for each set of analyses in DR Table 6.

331 5. U-Pb GEOCHRONOLOGIC RESULTS

332 Results of our U-Pb geochronologic analyses are described below, keyed to the age
333 distributions for individual samples that are shown on Figures 5, 6, and 7. Figure 8 presents age
334 distributions for combined sets of samples. Age distributions from all of the samples are
335 compared statistically in DR Table 4 using the five metrics described above, and MDS plots are
336 shown in Figure 9.

337 We note that Rasmussen et al. (2020~~19~~) have reported a subset of the LA-ICPMS ages
338 presented herein. The ages reported in their study are for the grains selected for CA-TIMS
339 analysis, which in most cases are among the youngest grains in each of our samples (as
340 documented in Appendix 2). This strategy was followed assuming that these grains represent
341 the youngest age components in each sample, and accordingly provide the most useful
342 maximum depositional ages. The individual dates reported in the two studies are identical, but,
343 given the selection process noted above, the pooled ages reported by Rasmussen et al.
344 (2020~~19~~) are consistently younger than the pooled ages reported herein. A comparison of the
345 results of the two studies is summarized in Appendix 2. The discussions below are based on the
346 full set of ages from each sample.

347 Sample numbers are registered to the CPCP core (CPCP-PFNP13-1A) by the number of the core
348 run and segment (e.g., our sample number 383-2 is from CPCP-PFNP13-1A-383Y-2, which
349 specifies that the material is from run 383, segment 2). The part of each segment that was
350 collected for geochronologic analysis is specified in DR Table 1.

351 5.1 Coconino Sandstone

352 Our sample from quartz arenite of the lower Permian (Leonardian) Coconino Sandstone
353 (sample 390-1) yielded 285 acceptable ages (DR Table 3; Figure 4). Most grains belong to two
354 broad age groups of ~2.0-1.0 Ga and ~640-295 Ma. Individual age peaks are at 2712, 1898,
355 1746, 1646, 1497, 1432, 1347, 1162, 1038, 667, 612, 590, 552, 476, 430, 419, 391, 374, 355,
356 341, and 300 Ma.

357 5.2 Moenkopi Formation

358 Five samples from the Lower-Middle Triassic Moenkopi Formation have been analyzed (Fig. 2).
359 The lowest sample (383-2) is assigned to the Wupatki Member based on the red-brown
360 laminated mudstone to fine-grained sandstone lithology (Fig. 2; Table DR 1). The age
361 distribution from this sample is very similar to that found in underlying upper Paleozoic strata,
362 with two dominant age groups from ~2.2 Ga to 1.0 Ga and from ~680 Ma to 250 Ma (Fig. 5).
363 Although the preferred interpretation for this sample is that it belongs to the lowest part of the
364 Moenkopi Formation, an alternative is that the sample is late Paleozoic in age, and perhaps
365 correlative with fine-grained clastic strata (e.g., the Toroweap Formation) that regionally overlie
366 the Coconino Sandstone. In an effort to provide a comparison with underlying and overlying
367 strata, the results from this sample are shown on Figures 5 and 6. Additional studies of the

368 sampled horizon are needed to resolve whether this sample belongs to the Moenkopi
369 Formation or underlying upper Paleozoic strata.

370 The upper four samples (349-3, 335-1, 327-2, and 319-2) are all from sandstone, siltstone, and
371 mudstone of the Holbrook Member. These samples yield generally similar age distributions
372 (average KS-D values ~~CCC~~ of 0.1924; DR Table 4), with significant proportions of ~1.42 Ga, 650-
373 510 Ma, 290-270 Ma, and 250-235 Ma ages (Fig. 6). With ages from all four Moenkopi
374 Formation samples combined, PDP peak ages are 1420, 594, 543, 285, and 250 Ma (Fig. 8). ~~As
375 shown in Figures 9B and 9C, age distributions from the lower two samples (349-3 and 335-1)
376 and upper two samples (327-2 and 319-2) form two distinct groups. These clusters are also
377 apparent from CCC values of 0.83 and 0.24 for the lower and upper samples (respectively), in
378 comparison with a low average value (0.08) for comparison of the two sets with each other (DR
379 Table 4).~~

380 **5.3 Chinle Formation**

381 Twenty-three samples from the Mesa Redondo Member, Blue Mesa Member, Sonsela Member,
382 and Petrified Forest Member of the Chinle Formation have been analyzed (Fig. 2). Results from
383 each member are described separately below.

384 **5.4 Mesa Redondo Member**

385 One sample of sandstone from the Mesa Redondo Member (305-2) yields dominant age groups
386 of ~2.0-1.6 Ga, 1.44 Ga, 1.1-1.0 Ga, 750-500 Ma, and 450-300 Ma, and 290-220 Ma (Fig. 7), with
387 PDP peak ages of 1443, 1036, 618, 412, 323, 248, and 223 Ma. As reported in DR Table 4 and
388 shown on Figure 9B and 9C, the >240 Ma ages in this sample resemble ages in the underlying
389 Moenkopi Formation and Coconino Sandstone.

390 **5.5 Blue Mesa Member**

391 Three samples (297-2, 287-2, 261-1) of siltstone and mudstone from the Blue Mesa Member
392 yield similar results, with nearly identical <240 Ma ages and small but varying proportions of
393 ~1.64 Ga, 1.44 Ga, 1.1-1.0 Ga, 650-500 Ma, and 440-240 Ma ages (Figures 7 and 8). Both <240
394 Ma ages (Fig. 9A) and >240 Ma ages (Fig. 9C) differ from those in underlying strata of the Mesa
395 Redondo Member. Between 56% and 89% of the grains analyzed from these samples yield ages
396 between 232 and 210 Ma, with PDP peak ages of 221-220 Ma (Fig. 7; DR Table 6). With all three
397 samples combined, 62% of the ages are <240 Ma, and PDP peak ages are 1630, 1440, and 220
398 Ma (Fig. 8).

399 **5.6 Sonsela Member**

400 Twelve samples (243-3 to 158-2) from the Sonsela Member yield two different sets of age
401 distributions (Figures 7, 8, and 9; DR Table 3). The lower six samples (243-3 to 196-3), all
402 consisting of sandstone and subordinate siltstone (DR Table 1), yield small numbers of
403 Precambrian grains that are mostly ~1.65 and 1.44 Ga, with few ~1.1-1.0 Ga grains. These

404 samples yield between 53% and 79% ages <240 Ma, with most ages between 234 and 208 Ma,
405 and PDP peak ages of 221-218 Ma (Fig. 7). With ages from all six samples combined, 68% of the
406 grains are <240 Ma, and PDP peak ages are 1650, 1445, 1084, and 219 Ma (Fig. 8). Comparison
407 of age distributions (Figures 7 and 8), KS-D values (DR Table 4), and MDS patterns (Fig. 9)
408 suggests that the <240 Ma ages in lower Sonsela Member these strata are similar to
409 indistinguishable from <240 Ma ages in underlying Blue Mesa strata, whereas >240 Ma ages in
410 the two sets of samples are less similar due to the variability of ages from the three Blue Mesa
411 Member samples. Ages that are >240 Ma in these strata have even less similarity to ages from
412 the Mesa Redondo Member, Moenkopi Formation, and Coconino Sandstone (Fig. 9; DR Table
413 4).

414 The upper six samples from the Sonsela Member (195-2 to 158-2) consist mainly of sandstone
415 and subordinate siltstone (DR Table 1). All six samples yield a subordinate but consistent
416 proportion of Precambrian ages that are mostly ~1.43 and 1.1-1.0 Ga, with few 1.65 Ga grains
417 (Fig. 7). Grains with ages of <240 Ma comprise between 39% and 77% of the grains analyzed.
418 These ages are somewhat younger than in lower Sonsela Member samples, with PDP peak ages
419 of 217-214 Ma. With all six samples combined, 50% of the grains are <240 Ma, and PDP peak
420 ages are 1643, 1434, 1082, 256, and 215 Ma (Fig. 8).

421 Statistical analysis (MDS patterns in Figure 9 and KS-D values in DR Table 4) shows that the
422 <240 Ma ages in upper and lower Sonsela Member strata are significantly different, whereas
423 >240 Ma ages are less distinct. Exceptions to this are >240 Ma ages in sample 243-3 (lower
424 Sonsela Member), which resemble equivalent ages in strata of the upper Sonsela Member (Fig.
425 9C), and <240 Ma ages in sample 196-3, which share characteristics with strata of both the
426 upper and lower Sonsela Member (Fig. 9A). Ages from strata of the upper Sonsela Member
427 show even less overlap with ages from strata of the Blue Mesa Member and underlying units
428 (Fig. 9 and DR Table 4).

429 **5.7 Petrified Forest Member**

430 Seven samples (131-2 to 52-2) from the Petrified Forest Member were collected mainly from
431 claystone, mudstone, siltstone, and fine-grained sandstone, with only the lowest sample (131-
432 2) consisting of coarse-grained sandstone. The upper six fine-grained samples yield between
433 17% and 72% <240 Ma ages that are significantly younger than in underlying strata, with PDP
434 peak ages between 212 and 209 Ma. Ages that are >240 Ma in most of these samples differ
435 from equivalent ages in strata of the Blue Mesa Member and Sonsela Member, but overlap to
436 varying degrees with ages in strata of the Mesa Redondo Member, Moenkopi Formation, and
437 Coconino Sandstone (Fig. 9C; DR Table 4). With the six samples combined, 35% of the grains are
438 <240 Ma, and PDP peak ages are 1636, 1430, 1032, 629, 379, 287, and 209 Ma (Fig. 8). The
439 lowest sample (131-2), consisting of coarse-grained sandstone, differs from the other Petrified
440 Forest Member samples, with an age peak of 221 Ma, and a greater proportion (68%) of >240
441 Ma ages (Fig. 7). The <240 Ma ages are very similar to equivalent ages in strata of the lower
442 Sonsela Member (Fig. 9A; KS-D=0.1297), whereas >240 Ma ages are slightly more similar to

443 ages in the upper Sonsela Member ($\text{CCCKS-D}=0.1772$) than in the lower Sonsela Member (KS-
444 $\text{DCCC}=0.2259$) (Fig. 9C).

445 **5.8 Summary of Chinle results**

446 The patterns of LA-ICPMS ages described above suggest that the studied part of the Chinle
447 Formation comprises four different units, each of which has a distinct chronologic signature for
448 both <240 Ma and >240 Ma ages (Fig. 8). These chronostratigraphic units correspond to the
449 Mesa Redondo Member, Blue Mesa Member and lower part of the Sonsela Member, upper
450 part of the Sonsela Member, and Petrified Forest Member.

451 **6. U AND Th GEOCHEMISTRY OF CHINLE ZIRCON GRAINS**

452 In an effort to evaluate whether the Triassic zircon grains from the four chronostratigraphic
453 units also have distinct chemical signatures [following Riggs et al. (2012, 2016)], Figure 10
454 summarizes the U concentrations and U/Th values for Triassic zircon grains analyzed from each
455 unit. The patterns exhibited in these plots suggest that (1) zircon grains from the Mesa
456 Redondo Member are significantly different from zircon grains in overlying strata, (2) grains in
457 strata of the Blue Mesa Member and lower Sonsela Member differ from grains in overlying
458 strata of the upper Sonsela Member and Petrified Forest Member, and (3) grains in strata of the
459 upper Sonsela Member and Petrified Forest Member have distinctive and slightly different
460 bimodal patterns. Plots showing U concentrations and U/Th values for individual samples are
461 included in DR Table 3.

462 **7. PROVENANCE INTERPRETATIONS**

463 Detrital zircon geochronology has previously been used to reconstruct the provenance of
464 Permian and Triassic strata of the Colorado Plateau by Riggs et al. (1996, 2003, 2012, 2013,
465 2016), Dickinson and Gehrels (2003, 2008), Gehrels et al. (2011), Lawton et al. (2015), and
466 Marsh et al. (2019). The results of most of these ~~chronological~~~~geochronologic~~ studies, and a
467 large number of stratigraphically based analyses, have recently been summarized by Dickinson
468 (2018). The following sections compare our new results with this existing information.

469 The following comparisons are based in part on qualitative comparison of age distributions of
470 the strata that we have analyzed and of age distributions from five potential source areas
471 (summarized on Figure 3). As described by Gehrels (2000), such comparisons focus on the
472 degree to which two age distributions contain similar proportions of similar ages. Comparisons
473 are also based on the results of statistical analyses (DR Table 4) that compare our results with
474 the age distributions of possible source areas, and on graphic displays of these comparisons
475 using MDS plots (Fig. 9).

476 **7.1 Coconino Sandstone**

477 Lawton et al. (2015) and Dickinson (2018) suggest that lower Permian strata of the Colorado
478 Plateau comprise a regional blanket of eolian strata that was shed predominantly from the

479 Appalachian and/or Ouachita orogens, with increasing input in northern regions from local
480 basement rocks exposed in the Uncompahgre or Ute Uplift (Fig. 1). These interpretations are
481 supported by the age distributions shown on Figures 5 and 11, with southern strata (Coconino,
482 Cedar Mesa, and White Rim sandstones) forming a distinct group dominated by
483 Appalachian/Ouachita detritus, and northern strata (Castle Valley and Cutler strata) forming a
484 separate group with increasing proportions of ca 1.44 Ga grains. The age distribution from our
485 Coconino Sandstone sample (390-1) fits well with other strata from the southern Colorado
486 Plateau in having abundant 1.2-1.0 and 670-300 Ma (Appalachian-Ouachita) grains and a low
487 proportion of ~1.44 Ga grains (Figures 5 and 11; DR Table 4).

488 7.2 Moenkopi Formation

489 As summarized on Figure 6, the detrital zircon ages from our four Holbrook Member samples
490 are generally similar to ages from a Holbrook Member sandstone reported by Dickinson and
491 Gehrels (2008). Dominant >300 Ma age groups and interpreted source terranes include ~1.44
492 Ga and subordinate ~2.0-1.6 Ga grains derived from Laurentian Precambrian basement and
493 ~670-300 Ma grains derived from Ouachita/Gondwana sources. Based on comparison with
494 detrital zircon ages from strata that accumulated in proximity to the East Mexico and southern
495 Cordilleran arcs (Fig. 3), 300-260 Ma grains (PDP peak ages of 285, 284, 265, 260, and 279) are
496 interpreted to have been shed from the East Mexico arc (peak age of 284 Ma), whereas 260-
497 230 Ma grains (peak ages of 250, 248, 228, 245, and 239 Ma) were likely shed from Early-
498 Middle Triassic parts of the Cordilleran magmatic arc in California and northwestern Mexico
499 (peak ages of 243, 236, and 226 Ma) (Fig. 3). Statistical analyses (DR Table 4) suggest nearly
500 equal contributions from the Ouachita orogen, local basement rocks, and the East Mexico arc.

501 More detailed analysis of the age distributions (Fig. 6) and MDS patterns (Fig. 9) suggest that
502 the lower two samples (349-3 and 335-1) [plus sample CP8 of Dickinson and Gehrels (2008)] are
503 dominated by ~1.44 Ga and ~285 Ma grains, whereas the upper two samples (327-2 and 319-2)
504 are dominated by ~620-590 Ma and ~250-230 Ma grains. The age distributions (Fig. 6) and
505 comparison metrics (Fig. 9C; DR Table 4) suggest that the lower samples were shed mainly from
506 local basement rocks (CECKS-D=0.350) and the East Mexico arc (CCC=0.22), whereas the upper
507 samples were shed largely from the Ouachita orogen (CECKS-D=0.23).

508 7.3 Chinle Formation

509 Our results from detrital zircon grains recovered from strata of the Chinle Formation are
510 consistent with the provenance and paleogeographic reconstructions offered by Riggs et al.
511 (1996, 2003, 2012, 2013, 2016), Dickinson (2018), and Marsh et al. (2019). Given the observed
512 age distributions (Fig. 7) and the location of our study site relative to Late Triassic
513 paleogeographic and paleotectonic features of southwestern North America (Fig. 12), likely
514 sources for pre-Triassic grains include rocks exposed in the Ouachita orogen to the southeast
515 and the Ancestral Mogollon highlands to the south and southwest. Given the abundance of ash
516 layers, bentonitic mudstone, and near-depositional-age zircon grains in strata of the Chinle

517 Formation, and the existence of arc-related plutons and volcanic rocks of Triassic age in Sonora
518 and southern California (Barth and Wooden, 2006, 2011, 2013; Saleeby and Dunne, 2015; Riggs
519 et al., 2016), Stewart et al. (1986), Riggs et al. (2012, 2016), Dickinson (2018), Marsh et al.
520 (2016), and many other researchers conclude that Triassic grains in Chinle strata were derived
521 from the active arc built along the southern Cordilleran margin. The occurrence in fore-arc and
522 back-arc strata of very similar distributions of ages (Fig. 3) is inconsistent with interpretations
523 (e.g., Hildebrand, 2009, 2013) that the early Mesozoic arc was located far from southwestern
524 North America.

525 Although our data are entirely consistent with the provenance interpretations outlined above,
526 the density of our sampling and the large number of analyses from most samples provide
527 opportunities to reconstruct temporal changes in Triassic provenance in greater detail, and with
528 the benefit of statistical analyses to quantify conclusions. Following are interpretations based
529 on strata belonging to each of the different members of the Chinle Formation.

530 **7.4 Mesa Redondo Member**

531 The provenance of strata belonging to the Mesa Redondo Member is similar to that of the
532 underlying Moenkopi Formation, with our sample (305-2) containing abundant ~640-300 Ma
533 grains derived from Ouachita/Gondwana sources as well as ~290-260 Ma grains derived from
534 the East Mexico arc (Fig. 8). Statistical analysis confirms higher similarity of >240 Ma grains with
535 Ouachita sources (0.58) than with Appalachian (0.35) or local basement (0.15) sources (DR
536 Table 4). This sample also yields a significant proportion of Triassic ages that approximate the
537 depositional age for these strata (Fig. 7). These young grains, with a PDP age peak of 223 Ma,
538 are interpreted to have been transported primarily by aeolian processes from the active
539 magmatic arc to the west (Fig. 12). Statistical analysis demonstrates that the Triassic ages in
540 these samples are significantly different from ages in overlying strata (Fig. 9A) and that the
541 >240 Ma ages are similar to those in some strata of the Petrified Forest Member (Fig. 9C).

542 **7.5 Blue Mesa Member**

543 Our three samples from strata of the Blue Mesa Member yield a large proportion of Triassic
544 zircon grains (Figures 7 and 8) that were derived from the active Cordilleran magmatic arc to
545 the west (Fig. 12), and a small proportion of pre-240 Ma grains that were shed from local
546 basement rocks and the Ouachita and/or Appalachian orogens (Fig. 8). Statistical analysis
547 confirms that the Triassic ages in all these samples are quite similar (Fig. 9A), whereas the age
548 distributions of >240 Ma grains in the three samples are more variable (Fig. 9C; DR Table 4).

549 **7.6 Lower Sonsela member**

550 The lower six samples from the Sonsela Member yield a large proportion of Triassic grains
551 derived from the Cordilleran magmatic arc, and fewer ages derived from local basement rocks
552 and Ouachita/Gondwana sources (Figures 7 and 8). Distinctive among the older grains is a
553 significant proportion of ~1.44 Ga grains that most likely may have been incorporated during

554 ~~transport from the Ouachita orogenic highlands, or may~~ signal increased input from the
555 Ancestral Mogollon highlands to the southwest (Marsh et al., 2019) (Fig. 12). MDS analysis
556 demonstrates that the <240 Ma and >240 Ma ages in these samples are quite similar, with the
557 ~~only significant~~ main difference being the larger number of ~1.1 Ga grains in sample 243-3
558 (Figures 7 and 9C).

559 **7.7 Upper Sonsela Member**

560 The upper six samples from the Sonsela Member reveal a continued low contribution from the
561 Ouachita orogen, and a significant increase in the proportion of ~1.08 Ga and 260-240 Ma
562 grains (Figures 7 and 8). The ~260-240 Ma grains were likely derived from Permian-Early Triassic
563 igneous rocks along the southern Cordilleran margin (Saleeby and Dunne, 2015; Riggs et al.,
564 2016), exposed in the Ancestral Mogollon Highlands (Fig. 12). The prominent ~1.44 and 1.08 Ga
565 grains in these samples may also have been shed from highland sources to the south and
566 southwest. Triassic grains in these samples record a slightly younger (230 to 204 Ma, peak age
567 of 215 Ma) phase of magmatism along the Cordilleran margin. Significant changes in both <240
568 Ma and >240 Ma ages occur between samples 196-3 and 195-2 (Figure 7). MDS analysis
569 demonstrates that patterns of both <240 Ma and >240 Ma ages are consistent among the six
570 upper Sonsela Member samples, but are distinct from ages in all other parts of the Chinle
571 Formation (Figures 7 and 9).

572 **7.8 Petrified Forest Member**

573 Strata of the Petrified Forest Member record an important shift in provenance, with
574 significantly greater detrital input from the East Mexico arc (~287 Ma) and the Ouachita orogen
575 (~640-300 Ma), and a broader range of >1.0 Ga basement sources (Figures 7 and 8). Triassic
576 grains in these strata are also significantly younger, with ages of 228 to 200 Ma (peak age of
577 209 Ma).

578 An exception to these patterns is recorded by ages from the coarse-grained sandstone of
579 sample 131-2, which has Precambrian grains that are mainly ~1.1-1.0 and 1.44 Ga (like upper or
580 lower Sonsela Member; Fig. 9CB), and Triassic grains that are ~221 Ma (like strata of the lower
581 Sonsela Member and Blue Mesa Member; Fig. 9A). This lower Petrified Forest Member sample
582 is interpreted to have been reworked mainly from lateral equivalents of underlying strata of the
583 Sonsela Member and Blue Mesa Member, with little or no input from the active arc to the west.
584 ~~MDS analysis shows that sample 116-1 contains a mix of these older reworked grains and the~~
585 ~~younger grains present in overlying strata (Fig. 9A).~~

586 **8. MAXIMUM DEPOSITIONAL AGES**

587 The depositional age of Triassic strata on the Colorado Plateau is of considerable interest
588 because of the rich faunal and paleoclimatic records preserved within the Moenkopi Formation
589 and Chinle Formation, and as the zircon-based geochronological framework for the early
590 Mesozoic when coupled with paleomagnetic polarity stratigraphy and astrochronology (Olsen

591 et al., 2018, 2019; Kent et al., 2018, 2019; Rasmussen et al., 202019). There accordingly have
592 been many prior attempts to determine the depositional age of these strata by dating igneous
593 zircon grains in ash beds or volcanic cobbles and detrital zircon grains in clastic strata (e.g.,
594 Riggs et al., 1996, 2003, 2012, 2013, 2016; Heckert et al., 2009; Dickinson and Gehrels, 2009;
595 Irmis et al., 2011; Ramezani et al., 2011, 2014; Atchley et al., 2013; Nordt et al., 2015). As part
596 the Colorado Plateau Coring Project, Kent et al. (2018) and Rasmussen et al. (202019) report
597 the results of CA-TIMS analyses on many of the same samples reported herein. All of the
598 available CA-TIMS ages, and the preferred age models of Kent et al. (2019) and Rasmussen et al.
599 (202019), are shown on Figure 13.

600 ~~Maximum depositional ages (MDA's) have been estimated calculated from the LA-ICPMS ages~~
601 ~~using four different methods (described above), with results presented in DR Tables 3 and 6 and~~
602 ~~shown graphically on Figure 13. We use the average of the youngest probability peak, tuffzirc,~~
603 ~~unmix, and weighted mean results to estimate the age of all dates belonging to the youngest~~
604 ~~cluster. In the following discussion we assume that the average of the ages and uncertainties~~
605 ~~calculated using these four different methods yields the most reliable maximum depositional~~
606 ~~age available from our LA-ICPMS data. These average (or preferred) ages are reported in DR~~
607 ~~Table 6, shown on Figure 13, and described below with 2 σ uncertainties incorporating only~~
608 ~~internal contributions (for inter-sample comparison) and incorporating both internal and~~
609 ~~external uncertainty contributions (for comparison with ages from other studies) (e.g., 224.4 \pm~~
610 ~~2.0/2.7 Ma).~~

611 Maximum depositional ages (MDA's) have been determined using the minimum age model of
612 Vermeesch (2020). The possibility that ~~this estimated~~ a maximum depositional age has been
613 compromised by Pb loss is evaluated mainly by determining whether there is a correlation
614 between U concentration and age. One criterion is whether the youngest single age has higher
615 U concentration than the average of the youngest cluster – if yes than the youngest analysis
616 (and perhaps other analyses within the youngest cluster) may have experienced Pb loss. A
617 second criterion is whether analyses within the youngest cluster display an inverse correlation
618 between U concentration and age – if yes, then the higher U and younger analyses within the
619 cluster may have experienced Pb loss. An additional criterion is whether the youngest date is
620 excluded from the cluster determined by Tuffzirc analysis. Samples in which all three methods
621 suggest the presence of Pb loss are shown with red arrows on Figure 13. Rasmussen et al.
622 (202019) document Pb loss in zircon grains from several of our samples by showing that CA-
623 TIMS ages are commonly older than LA-ICPMS ages from the same crystals.

624 ~~Evidence for Pb loss is shown on Figure 13 with small arrows adjacent to the MDA's, with the~~
625 ~~number of arrows showing the number of lines of evidence supporting Pb loss.~~

626 **8.1 Coconino Sandstone**

627 Our analyses do not provide a useful ~~MDA~~ maximum depositional age for strata of the Coconino
628 Sandstone (sample 390-1) because few late Paleozoic ages were recovered from this sample.

629 8.2 Holbrook Formation of the Moenkopi Formation

630 Of our four samples from the Holbrook Member of the Moenkopi Formation, three yield
631 ~~preferred~~MDA's that young upward from 24~~8.059-5~~ ($\pm 1.821-6/2-5$) Ma to 24~~6.638-4~~ (\pm
632 ~~1.922-0/2-8~~) Ma to ~~236.78245-7~~ ($\pm 9.921-9/2-7$) Ma (DR Table 6). These MDA's are consistent
633 with the inferred Early-Middle Triassic age of the strata and the corresponding ~251-237 Ma
634 range for Early and Middle Triassic time on the Geologic Time Scale (Cohen et al., 2013). All
635 three samples show patterns of U concentration that suggest the possibility of ~~minor~~Pb loss
636 (DR Table 6).

637 8.3 Mesa Redondo Member of the Chinle Formation

638 Our one sample (305-2) from strata of the Mesa Redondo Member yields an ~~n-preferred~~ MDA of
639 ~~223.243~~ $\pm 1.503/2-2$ Ma (DR Table 6). ~~s that all ages belong to the same age population, and~~
640 ~~p~~Patterns of U concentration do not indicate the presence of Pb loss (DR Table 6). This MDA
641 overlaps with CA-TIMS ages of ~224.7-221.7 Ma from the same sample but is ~~slightly~~ older than
642 the preferred single-grain age of ~221.7 Ma (Rasmussen et al., ~~2020~~2019). ~~However, t~~The LA-
643 ICPMS MDA of ~~223.243~~ $\pm 1.503/2-2$ is ~~significantly~~ younger than CA-TIMS ages of ~225.2 Ma
644 (Ramezani et al., 2011) and ~227.6 (Atchley et al., 2013) from outcrop samples of the Mesa
645 Redondo Member.

646 8.4 Blue Mesa Member of the Chinle Formation

647 Our three samples (297-2, 287-2, 261-1) from strata of the Blue Mesa Member yield ~~preferred~~
648 MDA's of ~~219.68220-6~~ $\pm 0.460-6/2-1$, ~~218.62220-2~~ $\pm 0.981-01-3/2-2$, and ~~2210.237~~ $\pm 1.021-3/1-9$
649 Ma (DR Table 6). All samples yield MSWD values >1.0 (average of 2.4), which indicates
650 ~~documents~~ the presence of multiple age populations ~~and/or Pb loss~~ (DR Table 6). Patterns of U
651 concentration suggest the ~~possible~~ presence of Pb loss in all three samples, ~~and likely Pb loss in~~
652 ~~sample 287-2~~. As shown on Figure 13, ~~these MDA's ages are slightly younger than similar to~~
653 ~~most~~ CA-TIMS ages ~~from strata of the Blue Mesa Member. From lower strata, our ages are~~
654 ~~slightly younger than a CA-TIMS age of~~ ~221.8 Ma [from sample 297-2; Rasmussen et al.
655 (20~~20~~19)], ~~and indistinguishable from a CA-TIMS age of~~ ~220.5 Ma [from sample 287-2;
656 Rasmussen et al. (20~~20~~19)], ~~and similar to an ID-TIMS age of~~ ~220.9 Ma [from outcrop; Heckert
657 ~~et al. (2009)~~]. From upper strata, our age is similar to a CA-TIMS age from outcrop of ~220.1 Ma
658 (Atchley et al., 2013) but significantly younger than a CA-TIMS age of ~223.0 Ma (Ramezani et
659 al., 2011), also from outcrop.

660 8.5 Lower part of the Sonsela Member

661 Our six samples from the lower part of the Sonsela Member (243-3 to 196-3) yield ~~preferred~~
662 MDA's of ~~219.27~~ $\pm 0.44220-3 \pm 0-9/1-8$ Ma (sample 243-3), ~~220.81~~ $\pm 0.44220-6 \pm 0-5/1-8$ Ma
663 (sample 227-3), ~~221.30~~ $\pm 0.48220-5 \pm 0-6/1-6$ Ma (sample 215-2), ~~219.21~~ $\pm 0.66220-9 \pm 0-7/2-3$ Ma
664 (sample 210-1), and ~~221.06~~ $\pm 0.50220-6 \pm 0-6/1-7$ Ma (sample 201-1). The sixth, uppermost
665 sample (196-3) yields younger ages with an ~~n-preferred~~ MDA of ~~217.93~~ $\pm 0.56218-2 \pm 0-7/1-6$ Ma.

666 MSWD values for these samples are all high (average of 2.6), which demonstrates the presence
667 of multiple age components. There is evidence for Pb loss in analyses from samples 243-3 and
668 210-1.

669 As shown on Figure 13, these MDA's are 1-3 m.y. older than most CA-TIMS ages from
670 equivalent strata. From oldest to youngest, the CA-TIMS ages include ~220.1 Ma [from outcrop;
671 Atchley et al. (2013)] from near the base, through ~218.8 Ma [sample 243-3; Rasmussen et al.
672 (202019)], ~217.7 Ma [sample 227-3; Rasmussen et al. (202019)], ~219.3 Ma [from outcrop;
673 Ramezani et al. (2011)], ~217.8 Ma [sample 215-2; Rasmussen et al. (202019)], ~218.0 Ma [from
674 outcrop; Ramezani et al. (2011)], and ~215.7 Ma and 214.4 Ma [samples 201-1 and 196-3;
675 Rasmussen et al. (202019)] at the top. The LA-ICPMS-based MDA's ages are also older than a
676 ~216.6 Ma MDA determined on LA-ICPMS ages from an outcrop sample of sandstone in the
677 middle part of the lower Sonsela Member, exposed ~132 km north of the CPCP core site (Marsh
678 et al., 2019).

679 **8.6 Upper part of the Sonsela Member**

680 The lower five samples from the upper Sonsela Member yield similar preferred MDA's of
681 214.36±0.68~~215.4 ± 1.1/2.2~~ Ma (sample 195-2), 216.32±0.72~~216.5 ± 0.7/1.9~~ Ma (sample 188-2),
682 216.19±0.62~~216.1 ± 0.9/2.1~~ Ma (sample 182-1), 214.81±0.70~~215.1 ± 0.8/1.9~~ Ma (sample 177-1),
683 and 217.07±0.86~~216.6 ± 1.0/2.0~~ Ma (sample 169-1). An upper sample yields a younger MDA of
684 214.18±0.54~~213.8 ± 0.6/2.1~~ Ma (sample 158-2). All samples yield MSWD values greater than 1.0
685 (average of 2.6) (DR Table 6), demonstrating the presence of multiple age components. Most
686 samples have patterns of U concentration that suggest the possibility of Pb loss. The lower five
687 MDA's are 2-3 m.y. older than CA-TIMS ages from equivalent strata, which include outcrop ages
688 of ~213.9 (Ramezani et al., 2011), ~213.6 Ma (Nordt et al., 2015), and ~213.1 Ma (Ramezani et
689 al., 2011), and CPCP core ages of ~214.0 Ma [samples 182-1 and 177-1; Rasmussen et al.
690 (202019)]. A CA-TIMS age of ~213.5 Ma for the upper sample [158-2; Rasmussen et al.
691 (202019)] is nearly identical to our age determination.

692 **8.7 Petrified Forest Member**

693 Our seven samples from the Petrified Forest Member yield three sets of ~~preferred~~ MDA's. The
694 lowest unit (sample 131-2) yields an MDA of 221.54±0.44~~221.5 ± 0.6/2.1~~ Ma, which is
695 significantly older than MDA's in adjacent strata. Four samples near the middle of the unit yield
696 similar ~~preferred~~ MDA's of 211.53±3.26~~211.5 ± 3.1/3.4~~ Ma (sample 116-1), 209.90±1.56~~211.6 ±~~
697 ~~1.7/2.5~~ Ma (sample 104-3), 210.42±1.08~~211.2 ± 1.2/1.9~~ Ma (sample 92-2), and
698 211.86±0.94~~211.7 ± 1.0/2.0~~ Ma (sample 84-2). These MDA's for two of these four samples
699 overlap with are very similar to an ID-TIMS age of ~211.9 Ma (Irmis et al., 2011) from equivalent
700 strata in outcrop, the other two younger MDA's may be compromised by Pb loss (Fig. 13).

701 Two upper samples, from the Black Forest bed, yield preferred MDA's of 208.26±3.38~~209.6 ±~~
702 ~~3.0/3.4~~ Ma (sample 66-1) and 209.75±0.42~~209.8 ± 0.5/1.6~~ Ma (sample 52-2). These MDA's are
703 similar to CA-TIMS ages of ~210.2 Ma from core [sample 52-2; Rasmussen et al. (202019)] and

704 ~209.9 Ma from outcrop (Ramezani et al., 2011), but are significantly younger than outcrop-
705 based ID-TIMS ages of ~211.0 Ma (Heckert et al., 2009) and ~213.0 Ma (Riggs et al., 2003). Most
706 of our samples yield MSWD values greater than 1.0 (average of 1.5), suggesting the presence of
707 multiple age components, and have patterns of U concentration that suggest the presence of
708 Pb loss.

709 9. COMPARISON OF LA-ICPMS, CA-TIMS, AND MAGNETOSTRATIGRAPHIC CONSTRAINTS ON 710 DEPOSITIONAL AGE OF CHINLE FORMATION STRATA

711 ~~Our preferred maximum depositional ages for strata of the Chinle Formation range from ~223.3~~
712 ~~to ~209.6 Ma, which is similar to the ~227.6 to ~209.9 Ma range of CA-TIMS ages (Fig. 13). All~~
713 ~~available U-Pb data therefore suggest that the analyzed Chinle Formation strata are Late~~
714 ~~Triassic, and probably Norian in age (Dickinson, 2018), given the assigned ages of ~237 to~~
715 ~~~201.3 for Late Triassic time (Cohen et al., 2013) and ~227 to ~208.5 Ma (Cohen et al., 2013) or~~
716 ~~~205.7 Ma (Kent et al., 2017) for Norian time.~~

717 ~~Figure 13 presents a comparison of our preferred maximum depositional ages, all available ID-~~
718 ~~and CA-TIMS ages [from Riggs et al. (2003), Heckert et al. (2009), Ramezani et al. (2011), Irmis~~
719 ~~et al. (2011), Atchley et al. (2013), Nordt et al., (2015), Kent et al. (2018), and Rasmussen et al.~~
720 ~~(2019)], and two age models that are based on magnetostratigraphic and CA-TIMS~~
721 ~~geochronologic information (Kent et al., 2019; Rasmussen et al., 2019). As shown on this figure,~~
722 ~~our LA-ICPMS MDA's overlap with most CA-TIMS ages and both age models for most strata~~
723 ~~belonging to the Blue Mesa Member and Petrified Forest Member, but are significantly older~~
724 ~~for strata of the Sonsela Member. The following discussion explores this pattern of~~
725 ~~convergence/divergence of the three chronometers — details of the magnetostratigraphic~~
726 ~~information, CA-TIMS data, and age models are discussed by Kent et al. (2018, 2019) and~~
727 ~~Rasmussen et al. (2019).~~

728 ~~Our preferred interpretation of the chronostratigraphic patterns is that U-Pb ages agree with~~
729 ~~magnetostratigraphic ages for strata containing abundant zircon crystals which are air-fall in~~
730 ~~origin, whereas U-Pb ages tend to predate deposition for strata that are dominated by zircon~~
731 ~~grains recycled from older units. The difference in proportion of air-fall (near-depositional-age)~~
732 ~~versus recycled (older) ages is interpreted to be controlled mainly by the grain size of the~~
733 ~~sedimentary host, which is important because only >60 µm zircon grains were analyzed in this~~
734 ~~study. Given that most detrital zircon grains transported with mud and silt are less than 60 µm~~
735 ~~in diameter, zircon grains analyzed from mudstone-siltstone samples (and sequences) are~~
736 ~~interpreted to be dominated by air-fall crystals rather than older recycled components. In~~
737 ~~contrast, because coarser grained sediment is able to transport >60 µm zircon grains,~~
738 ~~sandstone samples (and sequences) contain abundant recycled (older) zircon grains and a lower~~
739 ~~proportion of air-fall (near-depositional-age) zircon grains.~~

740 ~~Our LA-ICPMS ages from sandstones are significantly impacted by this difference because zircon~~
741 ~~grains were selected for analysis at random in an effort to generate an unbiased age~~

742 ~~distribution. CA-TIMS analyses from Chinle Formation sandstones have a higher yield of syn-~~
743 ~~depositional ages because zircon grains were selected for analysis on the basis of their juvenile~~
744 ~~appearance [e.g., acicular and prismatic crystals; Ramezani et al. (2011)] or from the youngest~~
745 ~~grains in an LA-ICPMS data set (e.g., Rasmussen et al., 2019; Appendix 2).~~

746 ~~These interpreted connections between stratigraphy, grain size, and proportions of air-fall~~
747 ~~versus recycled zircon grains lead to the interpretation that the three chronometric records~~
748 ~~agree (to within ~1 m.y.) for strata of the lower Blue Mesa Member and middle-upper Petrified~~
749 ~~Forest Member because these units are dominated by mudstone and siltstone, resulting in U-~~
750 ~~Pb ages mainly from air-fall (or slightly reworked) zircon grains. In contrast, LA-ICPMS ages from~~
751 ~~the Sonsela Member significantly pre-date deposition because the dominant sandstones~~
752 ~~contain abundant zircon grains recycled from slightly older units. For strata of the upper~~
753 ~~Sonsela Member, CA-TIMS ages approximate the true depositional age because the methods of~~
754 ~~grain selection were successful in identifying populations of air-fall zircon grains. For strata of~~
755 ~~the lower Sonsela Member, however, these methods were unsuccessful in identifying a~~
756 ~~sufficient number of air-fall zircon grains to determine a reliable depositional age, presumably~~
757 ~~because of their low abundance relative to recycled grains.~~

758 Our ~~preferred~~ maximum depositional ages for strata of the Chinle Formation range from
759 ~223.213 to ~208.39.76 Ma, which is similar to the ~227.6 to ~209.9 Ma range of CA-TIMS ages
760 (Fig. 13). All available U-Pb data therefore suggest that the analyzed Chinle Formation strata are
761 Late Triassic, and probably Norian in age (Dickinson, 2018), given the assigned ages of ~237 to
762 ~201.3 for Late Triassic time (Cohen et al., 2013) and ~227 to ~208.5 Ma (Cohen et al., 2013) or
763 ~205.7 Ma (Kent et al., 2017) for Norian time.

764 Figure 13 presents a comparison of our LA-ICPMS-based average ages and preferred maximum
765 depositional ages, all available ID- and CA-TIMS ages [from Riggs et al. (2003), Heckert et al.
766 (2009), Ramezani et al. (2011), Irmis et al. (2011), Atchley et al. (2013), Nordt et al., (2015), Kent
767 et al. (2018), and Rasmussen et al. (2020)], and two age models that are based on
768 magnetostratigraphic and CA-TIMS geochronologic information (Kent et al., 2019; Rasmussen et
769 al., 2020). As shown on this figure, our LA-ICPMS ages-MDA's reveal two first-order patterns.
770 The first pattern is that the LA-ICPMS-based ages-MDA's overlap with most CA-TIMS ages and
771 both age models for most strata belonging to the Blue Mesa Member and Petrified Forest
772 Member, but are significantly older for strata of the Sonsela Member. The second pattern is
773 that most LA-ICPMS-based ages-MDA's belong to five main clusters (~223 Ma, ~222-220 Ma,
774 ~217-215 Ma, ~212-211, and ~210 Ma), whereas the other chronologic records show a
775 relatively simple pattern of upward younging (Fig. 13). The following discussion explores these
776 two patterns – details of the magnetostratigraphic information, CA-TIMS data, and age models
777 are discussed by Kent et al. (2018, 2019) and Rasmussen et al. (2020).

778 As shown on Figure 13, the LA-ICPMS-based average ages and MDA's presented herein overlap
779 with the other chronometers for sequences which are dominated by fine-grained strata (e.g.,
780 Blue Mesa Member and Petrified Forest Member), but are several million years too old for

781 sequences which are dominated by coarse-grained strata (Sonsela Member) (Fig. 13). This
782 pattern appears to hold for member-scale stratigraphic units (e.g., strata from the Petrified
783 Forest Member), although some individual samples clearly do not follow this pattern. For
784 example, of the six samples from the Petrified Forest Member that yield LA-ICPMS
785 ~~ages~~maximum depositional ages which overlap with the other chronometers, four are
786 mudstone-siltstone and two are sandstone. In the lower Sonsela Member, of the six samples
787 ~~with that LA-ICPMS ages~~yield maximum depositional ages that predate the other
788 chronometers, five are sandstone and one is siltstone. These exceptions suggest that the
789 dominant lithic characteristics and depositional environment of a member (e.g., dominantly
790 fine-grained floodplain deposits for the Petrified Forest Member versus dominantly coarse-
791 grained channel deposits of the Sonsela Member [Woody, 2006]), are more important than the
792 grain size of an individual horizon in controlling the recognition of near-depositional-age zircon
793 grains.

794 The observed pattern that predominantly fine-grained strata of the Mesa Redondo, Blue Mesa,
795 and Petrified Forest members yield reliable LA-ICPMS ages~~MDA's~~, whereas predominantly
796 coarse-grained sandstones of the Sonsela Member do not, is surprising for two reasons. First, in
797 terms of provenance (as described above), strata of the Mesa Redondo, Blue Mesa, and
798 Petrified Forest members are interpreted to have been shed mainly from the Ouachita orogen,
799 which lacks Triassic igneous rocks, whereas strata of the Sonsela Member were shed from the
800 Cordilleran magmatic arc to the southwest, which contains abundant Permian and Triassic
801 igneous rocks (Fig. 3). Second, as shown in the margins of Figures 7 and 8, Triassic zircon grains
802 are significantly (~2x) more abundant in strata of the Sonsela Member than in underlying and
803 overlying strata. Based on these two observations, one might expect that strata of the Sonsela
804 Member would yield reliable MDA's, whereas strata from the Mesa Redondo Member, Blue
805 Mesa Member, and Petrified Forest Member would not.

806 We suggest that these counter-intuitive relations result in large part from our analytical method
807 of only analyzing zircon grains that are >60 um, combined with the maximum size of zircons
808 that can be transported in fine-grained versus coarse-grained sediments. For coarse-grained
809 sediment, >60 um zircon grains could include both transported (detrital) components that
810 predate deposition, as well as zircons that are air-fall in origin and approximately of
811 depositional age. A MDA calculated from a mix of these grains would accordingly pre-date
812 deposition. In contrast, Triassic zircon grains from fine-grained strata would tend to be mostly
813 air-fall in origin given that the older, transported grains are too small to analyze. An MDA
814 calculated from zircons that are primarily of air-fall origin would accordingly approach the true
815 depositional age.

816 The relations described above suggest that convergence versus divergence of the chronologic
817 records results from connections between depositional setting, grain size, provenance, and
818 analytical methods, which together conspire to control the proportions of air-fall (near-
819 depositional age) versus slightly older detrital zircon grains recognized in our samples. We

820 suggest that the three chronometric records agree (to within $\sim 1-2$ m.y.) for strata of the lower
821 Blue Mesa Member and middle-upper Petrified Forest Member because of the availability of
822 zircon grains of air-fall origin, which are near depositional age and both <60 μm and >60 μm in
823 size, versus the scarcity of pre-depositional-age Triassic grains of sufficient size for analysis due
824 to the lack of Triassic rocks in the source region (mainly the Ouachita orogen) and the small
825 (<60 μm) grain size of most sediment. In contrast, for the Sonsela Member, the LA-ICPMS
826 average ages and MDA's are interpreted to pre-date the other chronologic records because the
827 sediment was derived from the south, where abundant igneous rocks of Permian-Triassic age
828 were exposed, and the grain size of the detrital (pre-depositional-age) zircons was sufficiently
829 large that many would have been analyzed.

830 A test of this hypothesis is provided by MSWD values of the weighted means calculated for ages
831 from samples belonging to the various stratigraphic units. As shown in DR Table 6, average
832 MSWD values for samples from dominantly fine-grained strata of the Mesa Redondo-Blue Mesa
833 and Petrified Forest units are 1.7 and 1.3 (respectively), whereas coarser grained strata of the
834 lower and upper Sonsela units yield higher MSWD values of 2.6 and 2.1 (respectively). These
835 values are consistent with the interpretation that Triassic zircon grains in coarser-grained units
836 have a greater range of ages than Triassic zircon grains in finer-grained units.

837 These interpreted connections may also provide an explanation for the patterns of offset of the
838 CA-TIMS ages of Rasmussen et al. (2020) relative to the LA-ICPMS ages and
839 magnetostratigraphic age models in the Sonsela Member (Fig. 13). For strata of the upper
840 Sonsela Member, the CA-TIMS and magnetostratigraphic records converge because the
841 methods of grain selection were apparently successful in identifying populations of syn-
842 depositional age zircon grains. For strata of the lower Sonsela Member, however, these
843 methods were unsuccessful in identifying a sufficient number of depositional-age zircon grains
844 to determine a reliable MDA, presumably because of their low abundance relative to older
845 transported grains.

846 The second main pattern exhibited by the three chronometers is that most of the LA-ICPMS-
847 based average ages and MDA's belong to ~~five~~three main clusters (~ 223 Ma, $\sim 222-220$ Ma, $\sim 217-$
848 215 Ma, ~~and~~ $\sim 212-211$, and ~ 210 Ma), whereas the other chronologic records show a relatively
849 simple pattern of upward younging (Fig. 13). For the $\sim 222-220$ Ma cluster, a plausible
850 interpretation, following from the connections described above, is that $\sim 222-220$ Ma zircon
851 grains of air-fall origin accumulated in fine-grained strata of the lower Blue Mesa Member, and
852 were then recycled from age-equivalent strata into predominantly coarser grained channel
853 sands of the upper Blue Mesa Member and lower Sonsela Member. Grains from these same
854 sources appear to have also been recycled into sandstone sample 131-2 of the lower Petrified
855 Forest Member (Fig. 13). The $\sim 212-211$ Ma cluster may have formed in a similar fashion, with
856 initial accumulation of near-depositional-age air-fall zircons in mudstones of sample 116-1,
857 followed by recycling of these grains from age-equivalent strata into coarser-grained strata of
858 samples 104-3, 92-2, and 84-2 (Fig. 13).

859 The source of zircon grains that belong to the ~217-215 Ma cluster is less obvious given the lack
860 of recognized fine-grained strata dominated by zircons of this age (Fig. 13). One possibility is
861 that ~217-215 Ma grains were eroded from fine-grained strata exposed elsewhere [perhaps
862 near Sonsela Buttes (Marsh et al., 2019) or near the Cordilleran magmatic arc] that are
863 dominated by grains of this age. A second possibility is that fine-grained strata dominated by
864 ~217-215 Ma ages were originally present in the lower Sonsela Member, but were removed by
865 erosion and recycled into strata of the upper Sonsela Member. Previous workers have
866 suggested the existence of a hiatus or hiatuses (Ramezani et al., 2011) or an erosional event
867 (Rasmussen et al., 2020) at approximately this stratigraphic level, as shown by the preferred
868 age model of Rasmussen et al. (2020) on Figure 13. The occurrence of very different <240 Ma
869 ages, >240 Ma ages, and U/Th values in samples 196-3 and 195-2 suggests that this shift in
870 provenance, accumulation of a condensed section, or formation of an unconformity likely
871 coincides with the proposed boundary between strata of the lower Sonsela Member and upper
872 Sonsela Member. As discussed by Ramezani et al. (2011) and Rasmussen et al. (2020), the
873 possibility of an unconformity or condensed section near this stratigraphic position has
874 important implications for Chinle stratigraphy and fundamental Late Triassic biotic and climatic
875 changes. It should be noted, however, that no stratigraphic evidence for such an unconformity
876 was recognized in the CPCP core.

877 **10. IMPLICATIONS FOR THE STRATIGRAPHY OF THE CHINLE FORMATION**

878 The interpreted connections between the three geochronologic records and Chinle stratigraphy
879 provide an opportunity to reconstruct the depositional history of the Chinle Formation.
880 Fundamental assumptions in reconstructing this history are that:

881 (1) Chinle Formation strata encountered in the CPCP core record nearly continuous deposition
882 as described in the age model of Kent et al. (2019), perhaps with a period of erosion or very
883 slow deposition in the middle part of the Sonsela Member (Rasmussen et al., ~~2019~~2020).

884 (2) LA-ICPMS ages recovered from strata of the Chinle Formation belong to five separate groups
885 (red vertical bars of Figure 13) due to the hypothesized connections between stratigraphy, grain
886 size, and proportions of near-depositional-age (air-fall) versus older (recycled) zircon ages.

887 (3) Late Triassic igneous activity in the Cordilleran magmatic arc provided a nearly continuous
888 supply of zircon grains of air-fall origin to the Chinle deposystem. This assumption is supported
889 by the relatively continuous distribution of U-Pb ages within the Cordilleran magmatic arc and
890 back-arc (upper curves of Figure 13). ~~This view is in contrast to the hypothesis of Kent et al.~~
891 ~~(2019) that variations in the proportions of depositional-age versus older zircon grains result~~
892 ~~mainly from temporal changes in magmatic flux.~~

893 The interpreted stratigraphic evolution is summarized below and shown schematically on
894 Figure 14. Important phases in this evolution are as follows:

895 A: An LA-ICPMS MDA of ~223.3 Ma from our one sample from the Mesa Redondo Member
896 (305-2) agrees with the magnetostratigraphic information, the two age models, and the set of
897 CA-TIMS ages from this sample, presumably because these fine-grained strata are dominated
898 by zircon grains of air-fall origin. Older CA-TIMS ages of ~225.2 Ma (Ramezani et al., 2011) and
899 ~227.6 (Atchley et al., 2013) from outcrops of the Mesa Redondo Member may be
900 compromised by an abundance of recycled zircon grains.

901 B: LA-ICPMS average ages of ~221-220 Ma for most grains from fine-grained strata in the lower
902 part of the Blue Mesa Member are also near depositional age, presumably because the >60 um
903 zircon grains in these fine-grained strata are dominated by air-fall (or slightly reworked)
904 components. Minimum ages for these samples are somewhat younger, presumably due to Pb
905 loss.

906 C: LA-ICPMS ages from strata of the upper Blue Mesa Member significantly pre-date deposition,
907 presumably because these strata are dominated by recycled zircons. The predominance of
908 ~221-220 Ma LA-ICPMS MDA's ages suggests that most zircon grains were recycled from lateral
909 equivalents of underlying strata in the lower part of the Blue Mesa Member. CA-TIMS ages also
910 pre-date deposition, presumably because of the difficulty of isolating near-depositional-age
911 grains of air-fall origin.

912 D: This pattern continues up through most of the lower Sonsela Member, with LA-ICPMS
913 agesMDA's remaining at ~221-220 Ma (except where compromised by Pb loss) due to recycling
914 of strata from lateral equivalents of the lower Blue Mesa Member. Most CA-TIMS ages predate
915 the age of deposition because depositional-age (air fall) grains were diluted by recycled
916 components.

917 E: The age patterns from sandstones of the upper Sonsela Member are somewhat puzzling
918 given that the dominant ~217-215 Ma LA-ICPMS ages MDA's pre-date deposition, but fine-
919 grained strata that could have sourced grains of these ages are not present in the lower Sonsela
920 Member (Fig. 13). One possibility, as described above, is that the ~217-215 Ma grains were
921 eroded from fine-grained strata exposed elsewhere [~~perhaps near Sonsela Buttes~~ (Marsh et
922 al., 2019) or from the Cordilleran magmatic arc] that are dominated by grains of this age. A
923 second possibility is that fine-grained strata dominated by ~217-215 Ma ages were originally
924 present in the underlying lower Sonsela Member, but were removed by erosion and recycled
925 into strata of the upper Sonsela Member. An erosional event of the appropriate age and
926 stratigraphic position has been described by Ramezani et al. (2011) and by Rasmussen et al.
927 (202019), as shown by their age model on Figure 13. The occurrence of very different <240 Ma
928 ages, >240 Ma ages, and U/Th values in samples 196-3 and 195-2 suggests that this change in
929 provenance, condensed section, or unconformity most likely coincides with the boundary
930 between lower and upper Sonsela Member strata, ~~and perhaps with the red siliceous horizon~~
931 ~~recognized in the CPCP core.~~ As discussed by Rasmussen et al. (202019), the possibility of an
932 unconformity or condensed section near this stratigraphic position has important implications
933 for Chinle stratigraphy and fundamental Late Triassic biotic and climatic changes.

934 F: The dominance of pre-depositional-age grains in sample 131-2 provides strong evidence for
935 recycling of detrital zircons from lateral equivalents of underlying strata of the Blue Mesa
936 Member or lower Sonsela Member.

937 G: All chronometers agree for strata of sample 116-1, presumably because these fine-grained
938 strata are dominated by air-fall (or slightly reworked) detrital zircons.

939 H: LA-ICPMS ages MDA's from sandstones of the middle Petrified Forest Member (samples 104-
940 3, 92-2, and 84-2) slightly predate deposition (except where compromised by Pb loss) because
941 they were recycled from lateral equivalents of immediately underlying fine-grained strata (e.g.,
942 sample 116-1).

943 I: Most LA-ICPMS ages agree with the other All-chronometers agree for strata of the Black
944 Forest bed because this unit is dominated by air-fall (or slightly reworked) detrital zircon grains.
945 The minimum age for sample 66-1 is somewhat younger, presumably due to Pb loss.

946 **11. CONCLUSIONS**

947 First-order conclusions that result from our U-Pb geochronologic analyses of detrital zircon
948 grains from the Coconino Sandstone, Moenkopi Formation, and Chinle Formation are as
949 follows:

950 1. The provenance of strata belonging to the Coconino Sandstone and Moenkopi Formation can
951 be reconstructed by comparison of our LA-ICPMS ages (Figures 5 and 6) with age distributions
952 that characterize potential source regions (Figure 3). As shown on Figures 5 and 11, data from
953 our sample of the Coconino Sandstone and equivalent sandstones of the southern Colorado
954 Plateau suggest that these strata belong to an eolian blanket that was derived largely from the
955 Ouachita and/or Appalachian orogens, whereas strata from the northern Colorado Plateau
956 consist mainly of sediment derived from local basement uplifts (Fig. 1; Dickinson and Gehrels,
957 2003; Gehrels et al., 2011; Lawton et al., 2015). Lower-Middle Triassic strata of the Moenkopi
958 Formation record a very different dispersal system, with most detritus derived from the
959 Ouachita orogen, the East Mexico arc, and early phases of the Cordilleran magmatic arc (Figures
960 6 and 9).

961 2. LA-ICPMS ages from strata of the Chinle Formation belong to five groups that generally
962 correspond to the main stratigraphic units (Figures 7, 8, and 13). Maximum depositional ages
963 calculated from <240 Ma ages and provenance interpretations derived from >240 Ma ages are
964 as follows:

965 -- Strata of the Mesa Redondo Member yield a preferred MDA of ~223.3 Ma, and were derived
966 mainly from the Ouachita orogen.

967 -- Strata of the Blue Mesa Member yield MDA's of ~221.20.7 to ~218.620.2 Ma, and were
968 derived from local basement and Ouachita sources.

969 -- Strata in the lower part of the Sonsela Member yield similar MDA's of $\sim 221.30.9$ to
970 $\sim 219.220.3$ Ma (plus an uppermost sample with an MDA of $\sim 217.98.2$ Ma). Detritus was derived
971 mainly from local basement (especially ~ 1.44 Ga) sources, perhaps located in the ancestral
972 Mogollon highlands to the south.

973 -- Strata in the upper part of the Sonsela Member yield younger MDA's of $\sim 217.16.6$ to
974 $\sim 214.45.1$ Ma, plus an uppermost sample with an MDA of $\sim 214.23.8$ Ma. Grains with >240 Ma
975 ages were derived mainly from Precambrian basement (mainly ~ 1.44 Ga) and Grenville-age
976 rocks to south, as well as the East Mexico arc.

977 -- Strata of the Petrified Forest Member yield LA-ICPMS ages that belong to three separate
978 groups. The lowest sample yields an MDA of ~ 221.5 , which is significantly older than ages from
979 adjacent strata. The middle four samples yield MDA's of ~ 211.97 to $\sim 209.944.2$ Ma, whereas
980 the upper two samples yield MDA's of ~ 209.8 and $\sim 208.39.6$ Ma. All six upper samples contain
981 abundant >240 Ma grains that were shed from a broad range of Ouachita, local basement, and
982 East Mexico arc sources.

983 3. Patterns of U and Th concentration in Triassic zircon grains from the Chinle Formation belong
984 to four distinct groups that generally coincide with the chronostratigraphic units described
985 above. Changes in U and Th concentrations are interpreted to record variations in the chemistry
986 of arc magmatism through time, as has been documented previously by Barth and Wooden
987 (2006, 2011, 2013) and Riggs et al. (2010, 2012, 2016).

988 4. Comparison of the Chinle Formation MDA's with magnetostratigraphic information (Kent et
989 al., 2018, 2019) and CA-TIMS geochronologic information (Rasmussen et al., 202019) from the
990 CPCP core, plus CA-TIMS ages reported from outcrop samples, indicates that LA-ICPMS MDA's
991 approximate depositional ages for most strata of the Mesa Redondo Member, Blue Mesa
992 Member, and Petrified Forest Member (except where compromised by Pb loss), but
993 significantly pre-date deposition for strata of the Sonsela Member (Fig. 13). The correlation of
994 age patterns with stratigraphy is interpreted to reflect the proportions of air-fall (or slightly
995 reworked) versus recycled (older) zircon grains: fine-grained strata are dominated by near-
996 depositional ages because most zircon grains are air-fall (or slightly reworked) in origin,
997 whereas coarse-grained strata are dominated by pre-depositional ages because recycled zircon
998 grains dilute the abundance of air-fall crystals.

999 5. This hypothesized connection between stratigraphy and the three geochronologic records
1000 supports the following depositional history for Chinle Formation strata encountered in the CPCP
1001 core (Figures 13 and 14):

1002 -- LA-ICPMS ages and magnetostratigraphic information (Kent et al., 2019) indicate that the
1003 sampled part of the Mesa Redondo Formation was deposited at ~ 223.3 Ma. CA-TIMS ages of
1004 ~ 225.2 Ma (Ramezani et al., 2011) and ~ 227.6 (Atchley et al., 2013) from outcrop samples
1005 suggest that strata of the Mesa Redondo Member in other areas are dominated by older
1006 recycled components.

1007 -- Magnetostratigraphic information (Kent et al., 2019) suggests that strata of the Blue Mesa
1008 Member and lower Sonsela Member accumulated between ~222 Ma and ~214 Ma, whereas
1009 LA-ICPMS MDA's are consistently ~~~222-220~~ Ma for the same strata (except for the uppermost
1010 sample of ~~~217-218~~ Ma). This suggests that most zircons in strata of the upper Blue Mesa
1011 Member and lower Sonsela Member were recycled from lateral equivalents of strata of the
1012 lower Blue Mesa Member. The observation that most CA-TIMS ages from these strata also pre-
1013 date deposition is interpreted to result from the dilution of air-fall zircon crystals by older
1014 recycled zircon grains.

1015 -- Strata of the upper Sonsela Member accumulated between ~215 and ~213 Ma, as
1016 constrained by magnetostratigraphic information and CA-TIMS ages. LA-ICPMS MDAs from
1017 these strata are ~217-215 Ma, which indicates that they are dominated by zircons recycled
1018 from older units. The lack of samples in the lower Sonsela Member that are dominated by
1019 ~217-215 Ma grains suggests that zircon grains of this age in upper Sonsela Member strata may
1020 have been transported from sections of the Chinle Formation exposed outside of the PEFO
1021 area. It is also possible that such strata were exposed in the PEFO area, but were removed
1022 during an erosional event inferred by Rasmussen et al. (20~~2019~~) from the pattern of CA-TIMS
1023 ages in the upper Sonsela Member (Fig. 3). Significant changes in <240 Ma ages, >240 Ma ages,
1024 and U-Th values suggest that this unconformity, if present, occurs between samples 196-3 and
1025 195-2, ~~and may coincide with the red siliceous horizon recognized in the CPCP core.~~

1026 -- All available evidence suggests that mudstone and subordinate sandstone of the middle
1027 Petrified Forest Member accumulated at ~212-211 Ma, and the Black Forest bed in the upper
1028 part of the unit accumulated at ~210 Ma. In contrast, LA-ICPMS ages recovered from sample
1029 131-2, from the lower part of the Petrified Forest Member, are dominantly ~221 Ma, suggestive
1030 of recycling from lateral equivalents of strata of the Blue Mesa Member and lower Sonsela
1031 Member.

1032 6. Comparisons of our LA-ICPMS ages, the available CA-TIMS data, and magnetostratigraphic
1033 information provide insights into methods for determining the depositional age of fluvial strata.
1034 Our results show that the most reliable information comes from sequences dominated by fine-
1035 grained clastic strata (mudstone and siltstone) given that these strata have a low abundance of
1036 pre-depositional-age zircon grains of the appropriate size (>60 μm diameter) for routine
1037 analysis by LA-ICPMS. Mudstone-siltstone samples may accordingly ~~yield have~~ a high proportion
1038 of >60 μm zircon grains that are air-fall in origin (or only slightly reworked) and thereby record
1039 the age of deposition. In contrast, sedimentary sequences dominated by sandstone could well
1040 ~~commonly~~ yield abundant >60 μm zircon grains that predate deposition ~~have been recycled~~
1041 ~~from older sediments~~, thereby diluting syn-depositional-age zircon grains. Future attempts to
1042 determine depositional ages from fluvial strata should accordingly focus on sequences
1043 dominated by fine-grained strata, rather than sandstones, in spite of the challenges of
1044 extracting and analyzing the smaller zircon crystals.

1045

1046 **12. AUTHOR CONTRIBUTION**

1047 NG and GG generated the LA-ICPMS data reported in this paper. All coauthors were involved in
1048 acquiring the samples that were analyzed and/or interpreting the data. GG prepared this
1049 manuscript with input from all co-authors.

1050 **13. COMPETING INTERESTS**

1051 The authors declare that they have no conflict of interest.

1052 **14. ACKNOWLEDGEMENTS**

1053 Geochronologic analyses were conducted with support from NSF EAR-0959107 and EAR-
1054 1649254 (to Gehrels). Laboratory analyses were performed primarily by N. Giesler.
1055 Collaborative aspects of the project were supported by NSF EAR 0958976 (PEO & JWG),
1056 0958723 (RM), 0958915 (RBI), and 0958859 (DVK). Funding for coring and much logistical
1057 support was provided by ICDP (International Scientific Continental Drilling Program grant 05-
1058 2010: JWG, PEO, Jingeng Sha, Roberto Molina-Garza, Wolfram Kürschner, and Gerhard
1059 Bachmann). Additional funding was supplied by grants from the Lamont Climate Center (PEO).
1060 Field support was provided by LacCore personnel (Anders Noren, Kristina Brady, and Ryan
1061 O'Grady), drilling manager Doug Schnurrenberger, and core-handling volunteers (Justin Clifton,
1062 Bob Graves, Ed Lamb, Max Schnurrenberger, and Riley Black). Superintendent Brad Traver of
1063 the National Park Service arranged for permission to core in the PEFO and provided logistical
1064 support during site selection and drilling. This is Petrified Forest Paleontological Contribution 67.
1065 The conclusions presented here are those of the authors and do not represent the views of the
1066 United States Government.

1067 **REFERENCES CITED**

- 1068 Alsalem, O.B., Fan, M., Zamora, J., Xie, X., and Griffin, W.R.: Paleozoic sediment dispersal before
1069 and during the collision between Laurentia and Gondwana in the Fort Worth Basin, USA:
1070 *Geosphere*, v. 14, no. 1, p. 1–18, doi: 10.1130/GES01480.1, 2018.
- 1071 Ash, S.R.: The Black Forest Bed, a distinctive unit in the Upper Triassic Chinle Formation, north-
1072 eastern Arizona: *Journal of the Arizona-Nevada Academy of Science*, v. 24–25, p. 59–73, 1992.
- 1073 Atchley, S.C., Nordt, L.C., Dworkin, S.I., Ramezani, J., Parker, W.G., Ash, S.R., and Bowring, S.A.:
1074 A linkage among Pangean tectonism, cyclic alluviation, climate change, and biologic turnover in
1075 the Late Triassic: The Record from the Chinle Formation, Southwestern United States: *Journal of*
1076 *Sedimentary Research*, v. 83, p. 1147–1161, 2013.
- 1077 Baranyi, V., Reichgelt, T., Olsen, P.E., Parker, W.G., Kürschner, W.M.: Norian vegetation history
1078 and related environmental changes: new data from the Chinle Formation, Petrified Forest
1079 National Park (Arizona, SW USA): *Geological Society of America Bulletin*, v. 130, p. 775–795,
1080 doi.org/10.1130/B31673.1, 2017.
- 1081 Barth, A.P. and Wooden, J.L.: Timing of magmatism following initial convergence at a passive
1082 margin, southwestern US Cordillera, and ages of lower crustal magma sources: *Journal of*
1083 *Geology*, v. 114, p. 231–245, 2006.
- 1084 Barth, A.P., Walker, J.D., Wooden, J.L., Riggs, N.R., and Schweickert, R.A.: Birth of the Sierra
1085 Nevada magmatic arc: Early Mesozoic plutonism and volcanism in the east-central Sierra
1086 Nevada of California: *Geosphere*, v. 7, p. 877–897, 2011.
- 1087 Barth, A.P., Wooden, J.L., Jacobson, C.E., and Economos, R.C.: Detrital zircon as a proxy for
1088 tracking the magmatic arc system: The California arc example: *Geology*, v. 41, p. 223–226, 2013.
- 1089 Black, L., Kamo, S., Allen, C., Davis, D., Aleinikoff, J., Valley, J., Mundil, R., Campbell, I., Korsch,
1090 R., Williams, I., and Foudoulis, C.: Improved $^{206}\text{Pb}/^{238}\text{U}$ microprobe geochronology by the
1091 monitoring of a trace-element-related matrix effect; SHRIMP, ID–TIMS, ELA–ICP–MS and
1092 oxygen isotope documentation for a series of zircon standards: *Chemical Geology*, v. 205, p.
1093 115–140, 2004.
- 1094 Blakey, R.C., Peterson, F., and Kocurek, G.: Synthesis of late Paleozoic and Mesozoic eolian
1095 deposits of the western interior of the United States: *Sedimentary Geology*, v. 56, p. 3–125,
1096 1988.
- 1097 Chen, J.H., and Moore, J.G.: Uranium-lead isotopic ages from the Sierra Nevada batholith:
1098 *Journal of Geophysical Research*, v. 87, p. 4761–4784, 1982.
- 1099 Cohen, K.M., Finney, S.C., Gibbard, P.L., and Fan, J.-X.: The ICS International Chronostratigraphic
1100 Chart: Episodes v. 36, p. 199–204 (updated 2018), 2013.

1101 Creber, G.T., and Ash, S.R.: Evidence of widespread fungal attack on Upper Triassic trees in the
1102 southwestern U.S.A.: *Review of Palaeobotany and Palynology*, v. 63, p. 189-195, 1990.

1103 DeGraaff-Surples, K., Graham, S.A., Wooden, J.L., and McWilliams, M.O.: Detrital zircon
1104 provenance analysis of the Great Valley Group, California: Evolution of an arc-forearc system:
1105 *Geological Society of America Bulletin*, v. 114 (12), p. 1564–1580, 2002.

1106 Dickinson, W.R.: Tectonosedimentary Relations of Pennsylvanian to Jurassic strata on the
1107 Colorado Plateau, *Geological Society of America Special Paper 533*, 184 p., 2018.

1108 Dickinson, W.R., and Gehrels, G.E.: U-Pb ages of detrital zircon grains from Permian and Jurassic
1109 eolian sandstones of the Colorado Plateau, USA: Paleogeographic implications: *Sedimentary
1110 Geology*, v. 163, p. 29–66, 2003.

1111 Dickinson, W.R. and Gehrels, G.E.: U-Pb ages of detrital zircon grains in relation to
1112 paleogeography: Triassic paleodrainage networks and sediment dispersal across southwest
1113 Laurentia: *Journal of Sedimentary Research*, v. 78, p. 745–764, 2008.

1114 Dickinson, W.R. and Gehrels, G.E.: Use of U–Pb ages of detrital zircon grains to infer maximum
1115 depositional ages of strata: a test against a Colorado Plateau Mesozoic database: *Earth and
1116 Planetary Science Letters*, v. 288, p. 115–125, 2009.

1117 [Galbraith, R. and Laslett, G.: Statistical models for mixed fission track ages: Nuclear tracks and
1118 radiation measurements, v. 21 \(4\), p. 459-470, 1993.](#)

1119 Gehrels, G.E.: Introduction to detrital zircon studies of Paleozoic and Triassic strata in western
1120 Nevada and northern California, in Soreghan, M.J. and Gehrels, G.E., eds., *Paleozoic and Triassic
1121 paleogeography and tectonics of western Nevada and northern California: Geological Society of
1122 America Special Paper 347*, p. 1-18, 2000.

1123 Gehrels, G.E.: Detrital zircon U-Pb geochronology applied to tectonics: *Annual Review of Earth
1124 and Planetary Sciences*, v. 42, p. 127-149, 2014.

1125 Gehrels, G. and Pecha, M.: Detrital zircon U-Pb geochronology and Hf isotope geochemistry of
1126 Paleozoic and Triassic passive margin strata of western North America: *Geosphere*, v. 10 (1), p.
1127 49-65, 2014.

1128 Gehrels, G.E., Valencia, V., Pullen, A.: Detrital zircon geochronology by Laser-Ablation
1129 Multicollector ICPMS at the Arizona LaserChron Center, in Loszewski, T., and Huff, W., eds.,
1130 *Geochronology: Emerging Opportunities, Paleontology Society Short Course: Paleontology
1131 Society Papers*, v. 11, 10 p., 2006.

1132 Gehrels, G.E., Valencia, V., Ruiz, J.: Enhanced precision, accuracy, efficiency, and spatial
1133 resolution of U-Pb ages by laser ablation–multicollector–inductively coupled plasma–mass
1134 spectrometry: *Geochemistry, Geophysics, Geosystems*, v. 9, Q03017,
1135 doi:10.1029/2007GC001805, 2008.

- 1136 Gehrels, G., Blakey, R., Karlstrom, K., Timmons, M., Dickinson, W., and Pecha, M.: Detrital zircon
1137 U-Pb geochronology of Paleozoic strata in the Grand Canyon: *Lithosphere*, v. 3 (3), p. 183-200,
1138 2011.
- 1139 González-León, C.M., Valencia, V.A., Lawton, T.F., Amato, J.M., Gehrels, G.E., Leggett, W.J.,
1140 Montijo-Contreras, O., Fernández, M.A.: The lower Mesozoic record of detrital zircon U-Pb
1141 geochronology of Sonora, México, and its paleogeographic implications: *Revista Mexicana de*
1142 *Ciencias Geológicas*, v. 26 (2), p. 301-314, 2009.
- 1143 Heckert, A.B. and Lucas, S.G.: Revised Upper Triassic stratigraphy of the Petrified Forest
1144 National Park, Arizona, USA: *New Mexico Museum of Natural History Science Bulletin*, v. 21, p.
1145 1–36, 2002.
- 1146 Heckert, A.B., Lucas, S.G., Dickinson, W.R., and Mortensen, J.K.: New ID-TIMS U-Pb ages for
1147 Chinle Group strata (Upper Triassic) in New Mexico and Arizona, correlation to the Newark
1148 Supergroup, and implications for the “long Norian”: *Geological Society of America Abstracts*
1149 *with Programs*, v. 41, p. 123, 2009.
- 1150 Hildebrand, R.S.: Did westward subduction cause Cretaceous-Tertiary orogeny in the North
1151 American Cordillera?: *Geological Society of America Special paper* 457, 71 p., 2009.
- 1152 Hildebrand, R.S.: Mesozoic assembly of the North American cordillera: *Geological Society of*
1153 *America Special paper* 495, 169 p., 2013.
- 1154 Hoke, G., Schmitz, M., and Bowring, S.: An ultrasonic method for isolating nonclay components
1155 from clay-rich material: *Geochemistry Geophysics Geosystems*, v. 15, p. 492–498, 2014.
- 1156 Horstwood, M., Kosler, J., Gehrels, G., Jackson, S., McLean, N., Paton, C., Pearson, N., Sircombe,
1157 K., Sylvester, P., Vermeesch, P., Bowring, J., Condon, D., and Schoene, B.: Community-Derived
1158 Standards for LA-ICP-MS U-Th-Pb Geochronology – Uncertainty Propagation, Age Interpretation
1159 and Data Reporting: *Geostandards and Geoanalytical Research*, v. 40 (3), p. 311-332, 2016.
- 1160 Irmis, R.B., Mundil, R., Martz, J.W., and Parker, W.G.: High-resolution U-Pb ages from the Upper
1161 Triassic Chinle Formation (New Mexico, USA) support a diachronous rise of dinosaurs: *Earth and*
1162 *Planetary Science Letters*, v. 309, p. 258–267, 2011.
- 1163 Kent, D.V., Olsen, P.E., and Muttoni, G.: Astrochronostratigraphic polarity time scale (APTS) for
1164 the Late Triassic and Early Jurassic from continental sediments and correlation with standard
1165 marine stages: *Earth-Science Reviews*, v. 166, p. 153–180, 2017.
- 1166 Kent, D.V., Olsen, P.E., Rasmussen, C., Lepre, C.J., Mundil, R., Irmis, R.B., Gehrels, G.E., Giesler,
1167 D., Geissman, J.W., and Parker, W.G.: Empirical evidence for stability of the 405 kyr Jupiter-
1168 Venus eccentricity cycle over hundreds of millions of years: *Proceedings of the National*
1169 *Academy of Sciences*, v. 115, p. 6153–6158, 2018.

1170 Kent, D.V., Olsen, P.E., Lepre, C. Mundil, R., Rasmussen, C., Irmis, R.B., Gehrels, G.E., Giesler, D.,
1171 Geissman, J.W., Parker, W.G.: Magnetostratigraphy of the entire Chinle Formation (Norian age)
1172 in scientific drill core PFNP-1A from the Petrified Forest National Park (Arizona, USA) and
1173 implications for global correlations in the Late Triassic: *Geophysics, Geochemistry, Geosystems*
1174 (in review), 2019.

1175 Kissock, J.K., Finzel, E.S., Malone, D.H., and Craddock, J.P.: Lower–Middle Pennsylvanian strata
1176 in the North American midcontinent record the interplay between erosional unroofing of the
1177 Appalachians and eustatic sea-level rise: *Geosphere*, v. 14 (1), p. 141–161, 2018.

1178 Lawton, T.F., Buller, C.D., and Parr, T.R.: Provenance of a Permian erg on the western margin of
1179 Pangea: Depositional system of the Kungurian (late Leonardian) Castle Valley and White Rim
1180 sandstones and subjacent Cutler Group, Paradox Basin, Utah, USA: *Geosphere*, v. 11 (5), p. 1–
1181 32, 2015.

1182 Lucas, S.G.: The Chinle Group: revised stratigraphy and biochronology of Upper Triassic
1183 nonmarine strata in the western United States, in: *Aspects of Mesozoic Geology and*
1184 *Paleontology of the Colorado Plateau*, edited by: Morales, M., Museum of Northern Arizona
1185 Bulletin 59, Flagstaff: Museum of Northern Arizona Press, p. 27–50., 1993.

1186 Ludwig, K.R.: Isoplot 3.6: Berkeley Geochronology Center Special Publication 4, 77 p., 2008.

1187 Marsh, A.D., Parker, W.G., Stockli, D.F., and Martz, J.W.: Regional correlation of the Sonsela
1188 Member (Upper Triassic Chinle Formation) and detrital U-Pb zircon data from the Sonsela
1189 Sandstone bed near the Sonsela Buttes, northeastern Arizona, USA, support the presence of a
1190 distributive fluvial system: *Geosphere*, v. 15, <https://doi.org/10.1130/GES02004.1>, 2019.

1191 Martz, J.W. and Parker, W.G.: Revised lithostratigraphy of the Sonsela Member (Chinle
1192 Formation, Upper Triassic) in the southwestern part of Petrified Forest National Park, Arizona:
1193 *PLoS ONE* 5(2): e9329. doi:10.1371/journal.pone.0009329, 2010.

1194 Martz, J.W., Parker, W.G., Skinner, L., Raucchi, J.J., Umhoefer, P., and Blakey, R.C.: Geologic map
1195 of Petrified Forest National Park, Arizona: Arizona Geological Survey Contributed Map CM-12-A,
1196 1 map sheet, scale 1:50,000, 18 p., http://repository.azgs.gov/uri_gin/azgs/dlio/1487, 2012.

1197 Martz, J.W., Kirkland, J.I., Milner, A.R.C., Parker, W.G., Santucci, V.L.: Upper Triassic
1198 lithostratigraphy, depositional systems, and vertebrate paleontology across southern Utah:
1199 *Geology of the Intermountain West*, v. 4, p. 99-180, [https://www.utahgeology.org/wp-](https://www.utahgeology.org/wp-content/uploads/2018/05/GIW2017-v04-pp099-180-Martz.pdf)
1200 [content/uploads/2018/05/GIW2017-v04-pp099-180-Martz.pdf](https://www.utahgeology.org/wp-content/uploads/2018/05/GIW2017-v04-pp099-180-Martz.pdf), 2017.

1201 Miller, J.S., Glazner, A.F., Walker, J.D., and Martin, M.W.: Geochronologic and isotopic evidence
1202 for Triassic–Jurassic emplacement of the eugeoclinal allochthon in the Mojave Desert region,
1203 California: *Geological Society of America Bulletin*, v. 107, p. 1441–1457, 1995.

1204 Nordt, L., Atchley, S., Dworkin, S.: Collapse of the Late Triassic megamonsoon in western
1205 equatorial Pangea, present-day American southwest: *Geological Society of America Bulletin*, v.
1206 127 (11/12), p. 1798–1815, 2015.

1207 Olsen, P. E., Kent, D.V., and Whiteside, H.: Implications of the Newark Supergroup-based
1208 astrochronology and geomagnetic polarity time scale (Newark-APTS) for the tempo and mode
1209 of the early diversification of the Dinosauria: *Earth and Environmental Science Transactions of*
1210 *the Royal Society of Edinburgh*, v. 101, p. 201–229, 2011.

1211 Olsen, P., Geissman, J., Kent, D., Gehrels, G., and 23 others: Colorado Plateau Coring Project,
1212 Phase I (CPCP-I): a continuously cored, globally exportable chronology of Triassic continental
1213 environmental change from western North America: *Scientific Drilling*, v. 24, p. 15–40, 2018.

1214 Olsen, P.E., Laskar, J., Kent, D.V., Kinney, S.T., Reynolds, D.J., Sha, J. and Whiteside, J.H.:
1215 Mapping Solar System chaos with the Geological Orrery: *Proceedings of the National Academy*
1216 *of Sciences*, v. 116 (22), p. 10664-10673, 2019.

1217 Ortega-Flores, B., Solari, L., Lawton, T.F., and Ortega-Obregón, C.: Detrital-zircon record of
1218 major Middle Triassic–Early Cretaceous provenance shift, central Mexico: demise of
1219 Gondwanan continental fluvial systems and onset of backarc volcanism and sedimentation:
1220 *International Geology Review*, v. 56 (2), p. 237-261, 2014.

1221 Paces, J.B., & Miller, J.D.: Precise U-Pb ages of Duluth Complex and related mafic intrusions,
1222 northeastern Minnesota: Geochronological insights to physical, petrogenetic, paleomagnetic,
1223 and tectonomagmatic processes associated with the 1.1 Ga midcontinent rift system: *Journal of*
1224 *Geophysical Research*, v. 98 (B8), p. 13997–14013. <https://doi.org/10.1029/93JB01159>, 1993.

1225 Parker, W., and Martz, J.: Constraining the stratigraphic position of the Late Triassic (Norian)
1226 Adamanian-Revueltian faunal transition in the Chinle Formation of Petrified Forest National
1227 Park, Arizona: *Journal of Vertebrate Paleontology*, v. 29 (suppl. to 3), p. 162A, 2009.

1228 Parker, W.G., and Martz, J.W.: The Late Triassic (Norian) Adamanian–Revueltian tetrapod faunal
1229 transition in the Chinle Formation of Petrified Forest National Park, Arizona, *Earth and*
1230 *Environmental Science Transactions of the Royal Society of Edinburgh*: v. 101, p. 231–260,
1231 2011.

1232 Pipiringos, G.N., O’Sullivan, R.B.: Principal unconformities in Triassic and Jurassic rocks, Western
1233 Interior United States – a preliminary survey: *Geological Survey Professional Paper 1035-A*, 29
1234 p., 1978.

1235 Pullen, A., Ibanez-Mejia, M., Gehrels, G., Giesler, D., and Pecha, M.: Optimization of a Laser
1236 Ablation-Single Collector-Inductively Coupled Plasma-Mass Spectrometer (Thermo Element 2)
1237 for Accurate, Precise, and Efficient Zircon U-Th-Pb Geochronology: *Geochemistry, Geophysics,*
1238 *Geosystems*, v. 19. <https://doi.org/10.1029/2018GC007889>, 2018.

1239 Ramezani, J., Hoke, G.D., Fastovsky, D.E., Bowring, S.A., Therrien, F., Dworkin, S.I., Atchley, S.C.,
1240 and Nordt, L.C.: High precision U-Pb zircon geochronology of the Late Triassic Chinle Formation,
1241 Petrified Forest National Park (Arizona, USA): Temporal constraints on the early evolution of
1242 dinosaurs: *Geological Society of America Bulletin*, v. 123, p. 2142–2159, 2011.

1243 Ramezani, J., Fastovsky, D.E., and Bowring, S.A.: Revised chronostratigraphy of the lower Chinle
1244 Formation strata in Arizona Arizona and New Mexico (USA): high-precision U-Pb
1245 geochronological constraints on the Late Triassic evolution of dinosaurs: *American Journal of
1246 Science*, v. 314, p. 981–1008, 2014.

1247 Rasmussen, C., Mundil, R., Irmis, R.B., Geisler, D., Gehrels, G.E., Olsen, P.E., Kent, D.V., Lepre, C.,
1248 Geissmann, J.W., and Parker, W.G.: A high-resolution age model for the Upper Triassic Chinle
1249 Formation (Petrified Forest National Park, Arizona, USA) constrained by U-Pb geochronology
1250 and magnetostratigraphy: implications for Late Triassic paleoecological and
1251 paleoenvironmental change: *Geological Society of America Bulletin* (in review), 202019.

1252 Reichgelt, T., Parker, W.G., Martz, J.W., Conran, J.G., Cittert, J.H.A.K., Kürschner, W.M.: The
1253 palynology of the Sonsela Member (Late Triassic, Norian) at Petrified Forest National Park,
1254 Arizona, USA: *Review of Palaeobotany and Palynology*, v. 189, p. 18-28,
1255 doi.org/10.1016/j.revpalbo.2012.11.001, 2013.

1256 Riggs, N.R., Lehman, T.M., Gehrels, G.E., and Dickinson, W.R.: Detrital zircon link between
1257 headwaters and terminus of the Upper Triassic Chinle–Dockum paleoriver system: *Science*, v.
1258 273, p. 97–100, 1996.

1259 Riggs, N.R., Ash, S.R., Barth, A.P., Gehrels, G.E., and Wooden, J.L.: Isotopic age of the Black
1260 Forest Bed, Petrified Forest Member, Chinle Formation, Arizona: an example of dating a
1261 continental sandstone: *Geological Society of America Bulletin*, v. 115, p. 1315–1323, 2003.

1262 Riggs, N.R., Barth, A.P., González-León, C., Jacobson, C.E., Howell, E., Wooden, J.E., and Walker,
1263 J.D.: Provenance of Upper Triassic strata in southwestern North America as suggested by
1264 isotopic analysis and chemistry of zircon crystals, in Rasbury, E.T., Hemming, S., and Riggs, N.,
1265 eds., *Mineralogical and Geochemical Approaches to Provenance: Geological Society of America
1266 Special Paper 487*, p. 13–36, doi: 10.1130 /2012 .2487 (02), 2012.

1267 Riggs, N.R., Reynolds, S.J., Lindner, P.J., Howell, E.R., Barth, A.P., Parker, W.G., and Walker, J.D.:
1268 The Early Mesozoic Cordilleran arc and Late Triassic paleotopography: The detrital record in
1269 Upper Triassic sedimentary successions on and off the Colorado Plateau: *Geosphere*, v. 9, p.
1270 602–613, 2013.

1271 Riggs, N.R., Oberling, Z.A., Howell, E.R., Parker, W.G., Barth, A.P., Cecil, M.R., and Martz, J.W.:
1272 Sources of volcanic detritus in the basal Chinle Formation, southwestern Laurentia, and
1273 implications for the Early Mesozoic magmatic arc: *Geosphere*, v. 12, p. 439–463, 2016.

- 1274 Saleeby, J., and Dunne, G.: Temporal and tectonic relations of early Mesozoic arc magmatism,
1275 southern Sierra Nevada, California, in Anderson, T.H., Didenko, A.N., Johnson, C.L., Khanchuk,
1276 A.I., and MacDonald, J.H., Jr., eds., Late Jurassic Margin of Laurasia—A Record of Faulting
1277 Accommodating Plate Rotation: Geological Society of America Special Paper 513, p. 223–268,
1278 2015.
- 1279 Saylor, J.E., and Sundell, K.E.: Quantifying comparison of large detrital geochronology data sets.
1280 *Geosphere*12, 203–220, 2016.
- 1281 Saylor, J.E., Jordan, J.C., Sundell, K.E., Wang, X., Wang, S., and Deng, T.: Topographic growth of
1282 the Jishi Shan and its impact on basin and hydrology evolution, NE Tibetan Plateau: *Basin*
1283 *Research*, v. 30(3), p. 544-563, 2018.
- 1284 Stewart, J.H., Anderson, T.H., Haxel, G.B., Silver, L.T., and Wright, J.E.: Late Triassic
1285 paleogeography of the southern Cordillera: The problem of a source for the voluminous
1286 volcanic detritus in the Chinle Formation of the Colorado Plateau region: *Geology*, v. 14, p. 567–
1287 570, 1986.
- 1288 Sundell, K.E., Saylor, J.E., and Pecha, M.: Sediment provenance and recycling of detrital zircons
1289 from Cenozoic Altiplano strata in southern Peru and implications for the crustal evolution of
1290 west-central South America: *Journal of South American Earth Sciences*, (in review), 2019.
- 1291 Surpless, K.D., Graham, S.A., Covault, J.A., and Wooden, J.L.: Does the Great Valley Group
1292 contain Jurassic strata? Reevaluation of the age and early evolution of a classic forearc basin:
1293 *Geology*, v. 34 (1), p. 21–24, 2006.
- 1294 Thomas, W.A., Gehrels, G.E., Greb, S.F., Nadon, G.C., Satkoski, A.M., and Romero, M.C.: Detrital
1295 zircon grains and sediment dispersal in the Appalachian foreland: *Geosphere*, v. 13 (6), p. 2206-
1296 2230, 2017.
- 1297 Thomas, W.A., Gehrels, G.E., Lawton, T., Satterfield, J., Romero, M., and Sundell, K.: Detrital
1298 zircon grains and sediment dispersal from the Coahuila terrane of northern Mexico into the
1299 Marathon foreland of the southern Midcontinent: *Geosphere*, v. 16 (in press), 2019.
- 1300 Tobisch, O.T., Fiske, R.S., Saleeby, J.B., Holt, E., and Sorensen, S.S.: Steep tilting of metavolcanic
1301 rocks by multiple mechanisms, central Sierra Nevada, California: *Geological Society of America*
1302 *Bulletin*, v. 112 (7), p. 1043–1058, 2000.
- 1303 Vermeesch, P.: Multi-sample comparison of detrital age distributions: *Chemical Geology*, v. 341,
1304 p. 140-146, 2013.
- 1305 [Vermeesch, P.: Dissimilarity measures in detrital geochronology: *Earth-Science Reviews*, v. 178:](#)
1306 [p. 310–321, 2018a. doi: 10.1016/j.earscirev.2017.11.027.](#)
- 1307 [Vermeesch, P.: Statistics for fission tracks. In Malus´a, M. and Fitzgerald, P., editors, *Fission*](#)

1308 [track thermochronology and its application to geology. Springer, 2018b.](#)

1309 [Vermeesch, P.: Maximum depositional age estimation revisited: Geoscience Frontiers, in](#)
1310 [review.](#)

1311 Wissink, G.K., Wilkinson, B.H., and Hoke, G.D.: Pairwise sample comparisons and
1312 multidimensional scaling of detrital zircon ages with examples from the North American
1313 platform, basin, and passive margin settings: *Lithosphere*, <https://doi.org/10.1130/L700.1>,
1314 2018.

1315 Woody, D.T.: Revised stratigraphy of the lower Chinle Formation (Upper Triassic) of Petrified
1316 Forest National Park, Arizona: *Museum of Northern Arizona Bulletin*, v. 62, p. 17–45, 2006.

1317 Wright, J.E., and Wyld, S.J.: Alternative tectonic model for Late Jurassic through Early
1318 Cretaceous evolution of the Great Valley Group, California, in Cloos, M., Carlson, W.D., Gilbert,
1319 M.C., Liou, J.G., and Sorensen, S.S., eds., *Convergent Margin Terranes and Associated Regions:*
1320 *A Tribute to W.G. Ernst: Geological Society of America Special Paper 419*, p. 1-15, 2007.

1321 Xie, X., Anthony, J.M., and Busbey, A.B.: Provenance of Permian Delaware Mountain Group,
1322 central and southern Delaware basin, and implications of sediment dispersal pathway near the
1323 southwestern terminus of Pangea: *International Geology Review*, DOI:
1324 [10.1080/00206814.2018.1425925](https://doi.org/10.1080/00206814.2018.1425925), 2018.

1325 **FIGURE CAPTIONS**

1326 **Figure 1.** Map showing the main basement provinces of southern North America and Mexico.
1327 Also shown are locations of the study area within the Colorado Plateau, outlines of Ancestral
1328 Rocky Mountains uplifts, and the Permian-Triassic magmatic arc along the continental margin
1329 of southwestern North America. Modified from Gehrels et al. (2011).

1330 **Figure 2.** Strata encountered in the Colorado Plateau Coring Project (adapted from Olsen et al.,
1331 2018). Sampled horizons are shown relative to core depth, stratigraphic depth, and
1332 stratigraphic nomenclature relevant for the Petrified Forest region. Detailed descriptions of
1333 samples are provided in DR Table 1; images of the sampled material are presented in Appendix
1334 1.

1335 **Figure 3.** Normalized probability density plots of U-Pb (zircon) ages from source terranes.
1336 Distinctive age groups include 1750-1620 Ma and 1520-1360 Ma ages from southwest Laurentia
1337 basement provinces, 1240-960 Ma ages from Grenville-age provinces exposed in the
1338 Appalachian and Ouachita orogens, 640-570 Ma and 480-370 Ma ages characteristic of the
1339 Appalachian orogen, 670-300 Ma ages from the Ouachita orogen, 300-260 Ma ages from the
1340 East Mexico arc, and 260-200 Ma ages belonging to the Cordilleran magmatic arc of
1341 southwestern North America. See text for sources of information.

1342 **Figure 4.** Plot showing the accuracy of $^{206}\text{Pb}^*/^{238}\text{U}$ dates of secondary standards analyzed
1343 during the current study. Each pair of symbols represents the weighted mean age and 2σ
1344 uncertainty of R33 and FC-1 analyses conducted with each sample, expressed as % offset from
1345 reported ID-TIMS dates of 1099.9 Ma for FC-1 (Paces and Miller, 1993) and 419.26 Ma for R33
1346 (Black et al., 2004). For FC-1, 1065 analyses are reported, with MSWD = 0.95 for all analyses. For
1347 R33, 295 analyses are reported, with MSWD = 0.92 for all analyses. Data are reported in DR
1348 Table 7.

1349 **Figure 5.** Normalized probability density plots of detrital zircon ages from our sample of the
1350 Coconino Sandstone and from other lower Permian sandstones of the Colorado Plateau.
1351 Numbers of constituent analyses are shown for each sample. Data are from ¹Dickinson and
1352 Gehrels (2003), ²Gehrels et al. (2011), ³Lawton et al. (2015), and ⁴this study. Shown for
1353 reference are age ranges from the Appalachian orogen (purple bands) and from local basement
1354 rocks (blue bands) (from Figure 3), which are interpreted by previous researchers to have
1355 sourced most of the detritus in these units. Also shown is our sample 383-2, which is
1356 interpreted to belong to the Wupatki Member of the Moenkopi Formation, but has an age
1357 signature characteristic of lower Permian strata of the Colorado Plateau.

1358 **Figure 6.** Probability density plots of detrital zircon ages from four samples from the Moenkopi
1359 Formation (lower four curves) as well as a Moenkopi sample from Dickinson and Gehrels
1360 (2008). Numbers of constituent analyses are shown for each sample. Samples 349-3, 335-1,
1361 327-2, and 319-2, plus the sample from Dickinson and Gehrels (2008), are all from the Holbrook

1362 Member. Sample 383-2 is interpreted to belong to the Wupatki Member, but has an age
1363 distribution that resembles lower Permian strata. Source regions are interpreted to include
1364 local basement rocks (blue bands), the Ouachita orogen (green bands), the East Mexico arc (red
1365 band), and the Late Permian-Triassic arc built along the Cordilleran margin (orange band).

1366 **Figure 7.** Normalized probability density plots of detrital zircon ages from twenty-four samples
1367 from the Mesa Redondo, Blue Mesa, Sonsela, and Petrified Forest Members of the Chinle
1368 Formation. Numbers of constituent analyses are shown for each sample. Age distributions older
1369 than 240 Ma are exaggerated by 10x. Black tick marks indicate the interpreted maximum
1370 depositional ages for each sample (from DR Table 6). Source regions are interpreted to include
1371 local basement rocks (blue bands), the Ouachita orogen (green bands), the East Mexico arc (red
1372 band), and the Late Permian-Triassic arc built along the Cordilleran margin (orange band).
1373 Percent of all grains that are <240 Ma in age are shown for each sample on the left.

1374 **Figure 8.** Normalized probability density plots of detrital zircon ages from each set of samples
1375 analyzed in this study. Numbers of constituent analyses are shown for each sample. Age
1376 distributions older than 240 Ma for Chinle strata are exaggerated by 10x relative to <240 Ma
1377 ages. Age distributions for Moenkopi and Coconino Sandstones are exaggerated by 5x relative
1378 to Chinle ages. Source regions are interpreted to include local basement rocks (blue bands), the
1379 Ouachita orogen (green bands), the East Mexico arc (red band), and the Late Permian-Triassic
1380 arc built along the Cordilleran margin (orange band). Results from sample 383-2 are not
1381 included in this plot because of its uncertain stratigraphic position. Data from sample 131-2 are
1382 omitted because they differ from ages present in other samples from the Petrified Forest
1383 Member. Percent of all grains that are <240 Ma in age are shown for each sample on the left.

1384 **Figure 9.** MDS plot ([Vermeesch, 2013](#)) comparing age distributions of samples analyzed herein
1385 with each other and with possible source areas. MDS (metric) analyses ~~are based on the KS-D~~
1386 ~~values calculated from kernel density estimates of the age distributions~~ ~~cross-correlation~~
1387 ~~coefficient, and~~ were conducted using the software of Saylor et al. (2018). Data from samples
1388 analyzed herein are in DR Table 3. Ages for source regions are from the sources cited in the
1389 text. ~~Stars represent MDS values for sets of examples. Samples 383-2 with the exception that~~
1390 ~~sample 131 is not included with other Petrified Forest samples. Stars represent MDS values for~~
1391 ~~sets of examples, with the exception that sample 131-2 is not included with other Petrified~~
1392 ~~Forest samples.~~

1393 **Figure 10.** Density distributions of U concentration versus U/Th for Triassic grains in the four
1394 chronostratigraphic units recognized in this study. Plots made with Hf density plotter software
1395 of Sundell et al. (2019).

1396 **Figure 11.** MDS plot comparing age distributions of Permian strata of the Colorado Plateau with
1397 each other and with potential source regions including the Appalachian orogen, Ouachita
1398 orogen, and basement rocks of southwestern North America. Data sources are described in
1399 Figures 3 and 4. The data support the interpretation of Lawton et al. (2015) that the Coconino,

1400 Cedar Mesa, and White Rim sandstones (cool shades) belong to a regional blanket of eolian
1401 strata that was derived largely from the Appalachian and/or Ouachita orogen, where strata of
1402 the Castle Valley and Cutler formations (warm shades) include greater proportions of detritus
1403 derived from local basement sources.

1404 **Figure 12.** Sketch map of relevant tectonic features in southwestern Laurentia during Late
1405 Triassic time [adapted from Figure 42 of Dickinson (2018)].

1406 **Figure 13.** Plot showing the available chronologic information for strata of the Chinle Formation
1407 from the study area. LA-ICPMS results are shown using red crosses for interpreted maximum
1408 depositional ages [using the minimum age approach of Vermeesch (2020)], and various symbols
1409 for the four age estimates (and the average) of the youngest cluster. Red arrows indicate that
1410 LA-ICPMS ages may be compromised by Pb loss (DR Table 6). ~~interpreted maximum~~
1411 ~~depositional ages (and 2 σ uncertainties) for each sample, as determined by the four methods~~
1412 ~~described above and reported in DR Table 6. Preferred ages (vertical red lines) are the average~~
1413 ~~of the ages calculated by these four methods.~~ CA-TIMS and ID-TIMS ages are shown in
1414 approximate stratigraphic position (as shown by Kent et al., 2019), with outcrop samples in gray
1415 symbols and core samples using black symbols. Smaller symbols represent ID-TIMS ages or CA-
1416 TIMS ages based on a single age or of uncertain reliability. Stratigraphic units are keyed to
1417 dominant rock type, with brown = mudstone and siltstone, yellow = sandstone, pink =
1418 bentonite. Average grain size of each sample is shown with bars on left (from Appendix 1 and
1419 DR Table 1). PDP curves to right show 2.0 Ga to 240 Ma ages, as plotted on Figure 7. Also shown
1420 are age models of Kent et al. (2019) and Rasmussen et al. (202019). Vertical red bands show
1421 interpreted ages of main clusters of LA-ICPMS maximum depositional ages.

1422 Curves across top of diagram show the distribution of ages from (1) fore-arc strata of the
1423 Barranca and El Antimonio Groups in Sonora (Gonzalez-Leon et al., 2009; Gehrels and Pecha,
1424 2014) and the Great Valley Group in California (DeGraaff-Surpless et al., 2002; Surpless et al.,
1425 2006; Wright and Wyld, 2007), (2) Permian-Triassic igneous rocks in California (Chen and
1426 Moore, 2982; Miller et al., 1995; Tobisch et al., 2000; Barth and Wooden, 2006, 2011, 2013;
1427 Saleeby and Dunne, 2015), and (3) strata of the Chinle Formation in other parts of the Colorado
1428 Plateau (Dickinson and Gehrels, 2008; Riggs et al., 2012; Marsh et al., 2019). Diamond-shaped
1429 symbols beneath curves represent individual ages.

1430 **Figure 14.** Depositional model of strata of the Chinle Formation encountered in the CPCP core.
1431 Each time slice contains information about the dominant grain size of the host sedimentary
1432 rock, the abundance of syn-depositional-age zircon grains that are interpreted to be air-fall in
1433 origin, and the abundance of recycled zircon grains that pre-date deposition.